

https://dspace.org/

The lightning transient behaviour of a driven rod earth electrode in multi-layer soil

Nixon, Kenneth John

2007-03-07T13:11:44Z
http://hdl.handle.net/10539/2213

Downloaded from a DSpace repository. https://dspace.org/

THE LIGHTNING TRANSIENT BEHAVIOUR OF A DRIVEN ROD EARTH ELECTRODE IN MULTI-LAYER SOIL

Kenneth John Nixon

A thesis submitted to the Faculty of Engineering and the Built Environment, University of the Witwatersrand, Johannesburg, in fulfilment of the requirements for the degree of Doctor of Philosophy.

Johannesburg, July 2006

Declaration

I declare that this thesis is my own, unaided work, except where otherwise acknowledged. It is being submitted for the degree of Doctor of Philosophy in the University of the Witwatersrand, Johannesburg. It has not been submitted before for any degree or examination in any other university.

Signed this ____ day of _____ 20__

_____

Kenneth John Nixon

Abstract

The work presented extends and contributes to research in earthing and lightning protection and focuses on the transient behaviour of a driven rod earth electrode. Although previous work in this area has produced practical guidelines and models that may be used for lightning protection system design and analysis purposes, there has not been an investigation into the commonly encountered scenario of multiple layers of different soil types, particularly where high current densities cause ionisation to occur in the surrounding soil. In the research presented, the behaviour of a practical driven rod earth electrode subjected to peak impulse currents of up to 30 kA is analysed. Measurements obtained using a large-scale experiment arrangement are compared against results obtained using a time-domain circuit model simulation. It is shown that a single apparent resistivity value calculated from the steady state resistance equation and the measured steady state resistance can be used as a simplification for modelling the lightning current transient behaviour of a driven rod earth electrode in multi-layer soil. This represents a unique and valuable contribution to engineers working in the field of earthing and lightning protection.

Acknowledgements

I would like to acknowledge Professor Ian Jandrell and thank him for being a fantastic role model and source of inspiration for myself and countless others. I would also like to thank Professors Jan Reynders and George Gibbon for being superb mentors as well as for their encouragement and words of wisdom. I am particularly grateful for the invaluable experience gained through working on real earthing and lightning protection projects with Mr Ian McKechnie.

Funding and support from the following organisations is gratefully acknowledged:

- Eskom through the Tertiary Education Support Programme (TESP).
- The National Research Foundation (NRF) for supporting the High Voltage research programme at Wits.
- The Department of Trade and Industry (DTI) for Technology and Human Resources for Industry Programme (THRIP) funding.

Thanks are extended to the Electric Power Research Institute (EPRI) for providing the resources and for funding the large-scale testing at the Energy Delivery and Utilisation Centre, Lenox, Massachusetts, USA. Special thanks are extended to Dr Andrew Phillips for providing such a unique opportunity.

Finally, it is important to note that none of this would have been possible without the continual support and encouragement of my parents, family and friends. In particular, an extra big thank you is extended to my wife, Mia, for her patience, love and support.

Contents

Declaration i

Abstract ii

Acknowledgements iii

Contents iv

List of Figures viii

List of Tables x

List of Symbols xi

Nomenclature xiii

1 Introduction 1

2 Background 4

2.1 Previous Research 4

2.2 Assumptions and Limitations of Existing Models 5

2.3 Soil Ionisation for a Hemispherical Earth Electrode 7

2.4 Improved Models of Soil Ionisation 8

2.5 Dynamic Impedance of an Earth Electrode 10

2.6 Scope of the Thesis 10

3 Approach Taken **11**

3.1 Problem Statement 11

3.2 Overall Approach Taken 11

3.2.1 Circuit Model Simulation 12

3.2.2 Large-Scale Experiment 13

3.2.3 Earth Electrode and Soil Configuration 13

3.2.4 Impulse Current Waveshapes 14

3.3 Contribution of Thesis 15

4 Circuit Model Simulation **17**

4.1 Choice of Model 17

4.2 Derivation of the Model 18

4.2.1 Initial Assumptions Made 18

4.2.2 Determining the Effective Resistance of a Driven Rod 19

4.3 Algorithm and Implementation 20

4.3.1 Algorithm Describing the Model 22

4.3.2 Implementation Considerations 23

4.4 Simplified Soil Resistivity 23

4.5 Selection of Model Parameters 25

4.5.1 Choice of Ionisation and De-Ionisation Constants 25

4.5.2 Choice of Breakdown Strength of Soil 25

4.5.3 Choice of Soil Resistivity 25

4.6 Summary of the Circuit Model 25

5 Large-Scale Experiment **27**

5.1 Selection of Test Site 27

5.2 Overall Test Site 29

5.3 Impulse Generator 29

5.4 Test Electrode Configuration 30

5.5 Measurement Setup 30

5.5.1 Current Measurement 31

5.5.2 Voltage Measurement 31

5.6 Measurement Post-Processing 32

6 Comparison of Results and Discussion **33**

6.1 Comparison of Results 33

6.1.1 Summary 34

6.1.2 Current Waveshape 1 34

6.1.3 Current Waveshape 2 34

6.2 Discussion 37

6.3 Validity of the Simplification 38

7 Conclusion and Recommendations **39**

7.1 Conclusion 39

7.2 Recommendations for Further Research 39

A ATP-EMTP Source Code **41**

A.1 Introduction 41

A.2 Modified Liew-Darveniza Dynamic Model 41

A.3 ATP-EMTP circuit detail 44

A.4 Main Data Case File 45

B Modified Dynamic Impedance Model **47**

B.1 Modified Liew-Darveniza Model 47

B.2 Current Waveshapes Used for Comparison 48

B.3 Parameter Values 48

B.4 Results 49

B.5 Conclusion 51

C Measurement Considerations **52**

C.1 Measurement Challenges 52

C.2 Frequency Analysis of Measurement with Noise 53

C.3 Analysis of Voltage Measurement System 54

C.4 Filter Details 57

C.5 Raw and Filtered Experiment Data 57

C.6 Conclusion 60

References **61**

Bibliography **66**

List of Figures

2.1 Typical composition of soil. 5

2.2 Hemispherical earth electrode buried in homogeneous soil. 7

2.3 Soil ionisation zone surrounding a hemispherical earth electrode. . . 8

2.4 Illustrative profile of dynamic resistivity profile. 9

3.1 Earth electrode and multi-layer soil configuration considered. 14

3.2 Impulse currents used in large-scale experiment and simulations. . . 15

4.1 Simplified model for the impedance of a single driven rod showing the ionisation and de-ionisation zones. 19

4.2 Algorithm of model used to determine the effective dynamic resistance of driven rod electrode including the effect of soil ionisation. 21

4.3 Hemispherical earth electrode in multi-layer soil. 23

4.4 Equivalent circuit model implemented for simulation purposes. . . . 26

5.1 Photograph of test site. 28

5.2 Plan view of the test site showing key components of the experiment. 28

5.3 Equivalent circuit of the impulse generator and test setup. 29

6.1 Comparison of experiment and simulated results for current waveshape 1 – 4/10 μs, 5 kA and 29 kA. 35

6.2 Comparison of experiment and simulated results for current waveshape 2 – 6/14 μs, 7 kA and 29 kA. 36

6.3 Resistivity profile at a particular radius from the centre of the driven rod generated by the dynamic impedance model. 37

6.4 Discrete breakdown channels around an earth electrode. 38

A.1 Detail of the ATP-EMTP circuit used to generate the simulation results. 44

B.1 Illustrating the key difference between the modified and original Liew-Darveniza model. 48

B.2 Comparison of results obtained using modified and original Liew-Darveniza model. 50

C.1 Photographs of measurement equipment. 52

C.2 Measurement containing inductive ringing obtained by shorting out the earth electrode under test. 53

C.3 Photograph of high voltage measurement circuit. 54

C.4 High voltage impulse divider measurement circuit. 55

C.5 Normalised frequency response of voltage measurement system. . . . 56

C.6 Frequency response of filter used to remove unwanted signal. 57

C.7 Raw and filtered experiment data for current waveshape 1 – 4/10 μs, 5 kA and 29 kA. 58

C.8 Raw and filtered experiment data for current waveshape 2 – 6/14 μs, 7 kA and 29 kA. 59

List of Tables

3.1 Impulse current waveshapes. 14

4.1 Parameter values used in circuit model. 26

5.1 Summary of impulse generator parameters. 30

6.1 Summary of experiment and simulation results. 33

B.1 Current impulse waveshapes used for model comparison. 48

B.2 Parameter values used in models. 49

B.3 Comparison between Nixon's modified Liew-Darveniza model and Anderson's Liew-Darveniza model. 49

C.1 Summary of components in equivalent circuit of high voltage impulse divider measurement circuit. 56

List of Symbols

The principal symbols used in this thesis are summarised below. The units are shown in square brackets and the first equation where the symbol is used is given.

R_0	steady state resistance of a hemispherical electrode [Ω], *Equation (2.1)*
ρ_{soil}	soil resistivity [Ωm], *Equation (2.1)*
r_0	radius of hemispherical electrode [m], *Equation (2.1)*
J	current density [A/m^2], *Equation (2.2)*
I	magnitude of injected current [A], *Equation (2.2)*
r	radius of interest [m], *Equation (2.2)*
J_c	critical current density [A/m^2], *Equation (2.3)*
E_0	critical electric field (breakdown gradient) [V/m], *Equation (2.3)*
r_i	radius of soil ionisation zone [m], *Equation (2.4)*
ρ_i	Resistivity of soil ionisation zone [Ωm], *Equation (2.4)*
t	time [s], *Equation (2.5)*
$Z(t)$	dynamic impedance of earth electrode at time t [Ω], *Equation (2.5)*
$V(t)$	potential of earth electrode relative to true earth potential at time t [V], *Equation (2.5)*
$I(t)$	current flowing into earth electrode at time t [A], *Equation (2.5)*
a	radial distance from centre of earth electrode [m], *Equation (4.1)*

ρ_a	resistivity of elemental shell [Ωm], *Equation (4.3)*
da	thickness of elemental shell [m], *Equation (4.3)*
dR	resistance of elemental shell [Ω], *Equation (4.3)*
t_i	time since the onset of ionisation [s], *Equation (4.4)*
τ_i	ionisation time constant [s], *Equation (4.4)*
ρ_i	resistivity of ionisation zone [Ωm], *Equation (4.4)*
τ_d	de-ionisation time constant [s], *Equation (4.5)*
t_d	time measured from the onset of de-ionisation [s], *Equation (4.5)*
ρ_m	value of resistivity at onset of de-ionisation [Ωm], *Equation (4.5)*
ρ_d	resistivity of de-ionisation zone [Ωm], *Equation (4.5)*
R_{rod}	steady state resistance of a driven rod [Ω], *Equation (4.10)*
l_{rod}	length of driven rod earth electrode [m], *Equation (4.10)*
r_{rod}	radius of driven rod earth electrode [m], *Equation (4.10)*

Nomenclature

ATP-EMTP	Alternative Transients Program version of the Electromagnetic Transients Program
CIGRÉ	International Council on Large Electric Systems (Conseil International des Grands Réseaux Électriques)
IEC	International Electrotechnical Commission
IEEE	Institute of Electrical and Electronics Engineers
EPRI	Electric Power Research Institute
SABS	South African Bureau of Standards
SANS	South African National Standard
SPICE	Simulation Program with Integrated Circuit Emphasis
XLPE	Cross-linked polyethylene

Chapter 1

Introduction

An earth electrode is an important component in any electrical system because it protects both equipment and people from potentially hazardous voltages caused when lightning or fault currents are introduced into the system (SANS 10199, 2004). An earth electrode can take a variety of shapes and forms, and is typically installed in ground that has wide ranging characteristics. In South Africa, since a significant proportion of industry is located in areas characterised by dry, sandy or rocky ground with high resistivity values (Nixon, 1999) it is particularly important to understand the behaviour of an earth electrode, especially due to the unfavourably high lightning ground flash density also encountered in these areas (SANS 10313, 1999). Failure to correctly understand and quantify this behaviour inevitably results in the design of excessively expensive and/or ineffective earthing systems.

A commonly encountered scenario is an electrode that is installed in ground with various layers due to either geological stratification (IEEE Std 80, 2000; SANS 10199, 2004) or compacted back-fill on a new industrial site. Whilst the steady state behaviour of an earth electrode buried in homogeneous soil (IEEE Std 80, 2000; Phillips et al., 2004; SANS 10199, 2004; Sunde, 1949) and multi-layer soil (Chow et al., 1995; Dawalibi & Mukhedkar, 1974; Takahashi & Kawase, 1990) is well documented from both practical and theoretical perspectives, the non-trivial physical processes that occur during transient conditions are not yet fully understood and pose a considerable engineering challenge (Oettlé, 1987).

This thesis introduces a simplified yet still accurate engineering approach to modelling the lightning transient behaviour of a driven rod earth electrode buried in multi-layer soil. Using computer model simulations and large-scale experiment results the simplified approach is verified. Simulation results are obtained using transient analysis of an equivalent circuit that includes the non-linear effect of soil ion-

isation using a modified version of the Liew-Darveniza model (Liew & Darveniza, 1974; Nixon, 1999). The experiment results used are from a series of outdoor experiments where high current impulses were applied to a single driven rod earth electrode (Phillips & Anderson, 2002).

The structure of the thesis is as follows:

Chapter 2: A brief outline of previous research is provided. The assumptions and limitations of existing models are discussed. Fundamental principles are introduced by considering the transient behaviour of a hemispherical electrode. Improved soil ionisation models are summarised. The important concept of the dynamic impedance of an earth electrode is explained and the scope of the thesis is defined.

Chapter 3: The problem addressed by the thesis is defined and the overall approach taken to solve the problem is described. The earth electrode and soil configuration selected for investigation is explained as well as the choice of impulse current waveshapes. The contribution made by the thesis is provided.

Chapter 4: The equivalent circuit model used to simulate the non-linear behaviour of a driven rod earth electrode in multi-layer soil is described. The derivation, the algorithmic representation and subsequent implementation of the model are presented. The choice of parameter values used in the simulation is discussed, and in particular the use of a simplified value of soil resistivity is proposed.

Chapter 5: The selection of a suitable large-scale experiment test site used to apply high current impulses to a single driven rod earth electrode in multi-layer soil is discussed. Details are provided about the overall test site, including the impulse generator used, the current and voltage measurement setup and the necessary measurement post-processing employed.

Chapter 6: The simulation and experiment results obtained in **Chapters 4** and **5** are compared and discussed. It is shown that there is strong agreement between the simulated and experiment values supporting the simplified approach introduced by the thesis. Some thoughts on modelling and the validity of the simplification made to the value of soil resistivity used are presented.

Chapter 7: The findings of the thesis are summarised and areas for further research are identified.

Additional supporting material is provided in the appendices as follows:

Appendix A: The ATP-EMTP source code for the MODELS implementation of the dynamic resistance described in **Chapter 4** and the corresponding main data case file used to generate the simulation results in **Chapter 6** are provided.

Appendix B: The key modification introduced to the Liew-Darveniza model in **Chapter 4** is summarised. Using current waveshapes and parameter values similar to those used in body of the thesis the modified model is compared against an alternative implementation. It is shown that the modified model adequately describes the dynamic behaviour of a driven rod earth electrode.

Appendix C: The measurement challenges encountered in the experiment are discussed. The inadvertent resonance in the setup is characterised and its source explained. Details are provided on the filter used to remove the unwanted noise. The raw unfiltered and final filtered experiment data is presented.

For convenience, each chapter and appendix begins with a summary of the main points covered and each chapter ends with a brief introduction to the following chapter.

In the following chapter a background to the transient behaviour of an earth electrode is provided and an overview of previous work in the area is given.

Chapter 2

Background

A brief outline of previous research into the transient behaviour of an earth electrode is provided. The assumptions and limitations of existing models are discussed. Fundamental principles are introduced by considering the transient behaviour of a hemispherical electrode. Improved soil ionisation models are summarised. The important concept of the dynamic impedance of an earth electrode is explained. The scope of this thesis is defined.

2.1 Previous Research

Early research performed by Towne (1929) and Sunde (1940) revealed a marked difference between the transient and the steady state behaviour of an earth electrode. Further comprehensive experimental studies undertaken by Bellaschi et al. (1942) confirmed this observation for a range of soil types and electrode configurations. Since then, several researchers have developed models that account for this difference in behaviour (Chisholm & Janischewskyj, 1989; Geri, 1999; Korsuncev, 1958; Liew & Darveniza, 1974; Oettlé, 1988).

Recently it has become important to re-visit and further quantify this behaviour due to the growing need for safe and reliable power delivery, coupled with the increasing sensitivity of modern electronic equipment to damaging transients caused by lightning. This is particularly true in South Africa where there is not only a large electrification drive, but there is the challenge that the majority of the country's business and industry is located in areas with poor soil conditions (500 to 2000 Ωm) and relatively high average lightning ground flash densities (5 to 9 flashes per square

kilometre per year) (Nixon, 1999; SANS 10313, 1999). The direct economic influence that the transient behaviour of an earth electrode has in this context cannot be emphasised enough, since the beneficial effect of breakdown occurring in the surrounding soil is evident even for currents as low as 1 kA (Phillips et al., 2004).

Specific attention in previous research is usually given to transmission tower grounding (CIGRE WG 33:01, 1991; Oettlé, 1988; Phillips et al., 2004) since this has a significant effect on the lightning performance and effective operation of an electric power transmission system. On the other hand, the dynamic model originally proposed by Liew & Darveniza (1974), and subsequently modified by Nixon (1999) for use within a time-domain transient simulation, may be used for more comprehensive and general lightning performance studies. Common to all existing models, however, is the fact that several key assumptions need to be introduced to simplify modelling. Furthermore, the exact physical processes occurring in the soil are still not yet fully understood as explained in the following section.

2.2 Assumptions and Limitations of Existing Models

As illustrated in *Figure 2.1*, soil is typically composed of several different substances including, for example, water, pockets of air, gravel, sand, clay, dissolved gases, mineral salts and organic material (Oettlé, 1987). All these substances affect the electrical characteristics of the soil. Although the breakdown characteristics of the constituent solid, liquid and gaseous dielectrics are individually well understood (Kuffel et al., 2000), a comprehensive physical model to explain their combined behaviour has not yet been developed.

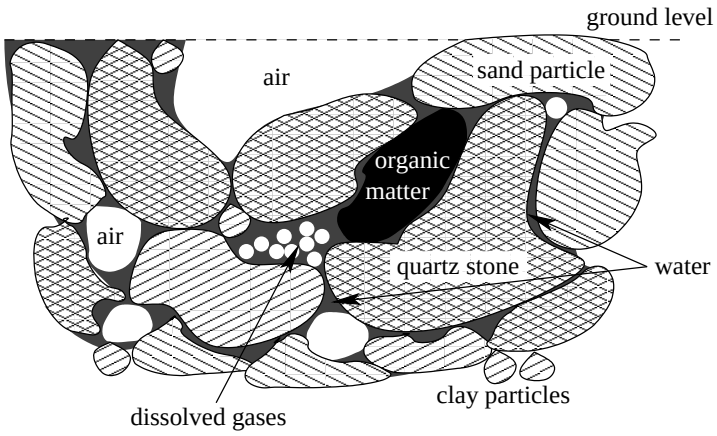

Figure 2.1: Typical composition of soil.

It is generally accepted that the electric field generated by high current densities results in discharge channels within the water and gas interfaces within the soil surrounding the electrode (Oettlé, 1987). Since the resistivity of the plasma in the discharge channels is lower than that of the surrounding soil there is an apparent decrease in the resistance to earth of the electrode. This effect is usually referred to as soil ionisation.

Three simplifications are commonly introduced when modelling the complicated scenario explained above (Mousa, 1994; Oettlé, 1988):

1. The soil is assumed to be uniform and homogeneous.
2. Breakdown in the surrounding soil is assumed to occur within a uniform zone.
3. Different types of soil are assumed to have the same dielectric strength regardless of moisture content or constituent components.

A fourth simplification often introduced is to completely ignore the effect of soil ionisation on the basis that the resulting model represents a conservative, or worst-case, scenario. In particular, rigorous electromagnetic transient simulations of earthing systems, based on frequency-domain analysis, do not account for soil ionisation since it is very difficult to include this non-linear effect (Dawalibi et al., 1995). Economically it is difficult to ignore the beneficial effect resulting from soil ionisation, especially since this effect is most marked for poor soil conditions such as those found in several regions of South Africa. Failure to account for the effect therefore results in expensive and inefficient earthing system designs.

Although the assumptions discussed above may seem unrealistic they nevertheless result in practical models that can be successfully used within engineering studies. More importantly, the fundamental parameters, for example moisture content, that influence the performance of an earth electrode (IEEE Std 80, 2000) vary so considerably that it is difficult to obtain accurate predictions and it is frequently better to consider the upper and lower limits of performance.

To introduce the fundamental principles and parameters involved in the non-linear transient behaviour of an earth electrode the next section considers the behaviour of a hemispherical electrode (CIGRE WG 33:01, 1991).

2.3 Soil Ionisation for a Hemispherical Earth Electrode

Consider a basic hemispherical electrode buried in homogeneous soil with a particular resistivity as shown in *Figure 2.2*. The steady state resistance of this electrode is given by (CIGRE WG 33:01, 1991):

$$R_0 = \frac{\rho_{soil}}{2\pi r_0} \tag{2.1}$$

where

R_0 = steady state resistance of a hemispherical electrode [Ω]
ρ_{soil} = soil resistivity [Ωm]
r_0 = radius of hemispherical electrode [m]

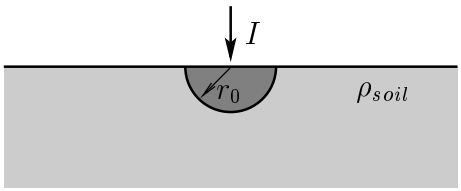

Figure 2.2: A perfect conducting hemispherical earth electrode of radius r_0 buried in homogeneous soil with resistivity ρ_{soil} and injected with current I.

When a given impulse current is injected into the electrode, the current density at a particular radius in the surrounding soil is given by (assuming a 1 m radius hemisphere):

$$J = \frac{I}{2\pi r^2} \tag{2.2}$$

where

J = current density [A/m^2]
I = magnitude of injected current [A]
r = radius of interest [m]

Soil ionisation is said to occur where the current density or the resulting electric field in the soil exceeds a particular threshold value given by:

$$J_c = \frac{E_0}{\rho_{soil}} \tag{2.3}$$

where

J_c = critical current density [A/m^2]
E_0 = critical electric field (breakdown gradient) [V/m]
ρ_{soil} = soil resistivity [Ωm]

Using *Equation (2.3)* the following equation can be used to show that the radius of the soil ionisation zone shown in *Figure 2.3* is given by:

$$r_i = \sqrt{\frac{\rho_{soil} I}{2\pi E_0}} \tag{2.4}$$

where

r_i = radius of soil ionisation zone [m]
ρ_{soil} = soil resistivity [Ωm]
I = magnitude of injected current [A]
E_0 = critical electric field (breakdown gradient) [V/m]

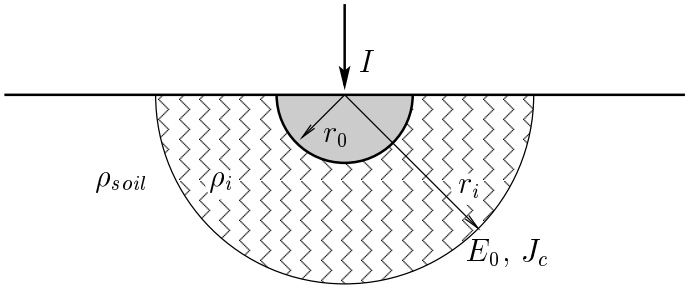

Figure 2.3: A perfect conducting hemispherical earth electrode of radius r_0 buried in homogeneous soil of resistivity ρ_{soil} and injected with current I. The resistivity of the ionisation zone is ρ_i and its radius r_i is governed by E_0 (J_c).

The previous derivation implicitly assumes ionisation occurs within a uniform zone around the earth electrode. Bellaschi et al. (1942) and Petropoulos (1948) proposed that the resistivity of this zone, ρ_i, instantaneously assumes the same value as that of the earth electrode. In other words, soil ionisation is modelled by an increase in the effective radius of the electrode. Given its simplicity, this model is frequently used to describe the behaviour of a driven rod in larger studies despite its lack of accuracy.

2.4 Improved Models of Soil Ionisation

Liew & Darveniza (1974) improved on the basic model described in the previous section by developing a model that introduced a dynamic resistivity profile as shown in *Figure 2.4*. In essence the model assumes that the resistivity of the soil at different radii from the earth electrode changes as a function of current and time. This model accounts for the intuitive physical time constants that are involved in the process. This model was modified and implemented in the Alternative Transients

Program version of the Electromagnetic Transients Program (ATP-EMTP)(Meyer & Liu, 1982) by Nixon (1999) enabling its use within larger comprehensive lightning protection studies. Further research performed by Yasuda et al. (2003) showed good agreement between this model and experiment results for currents up to 120 kA injected into the tower footing of a 500 kV transmission line.

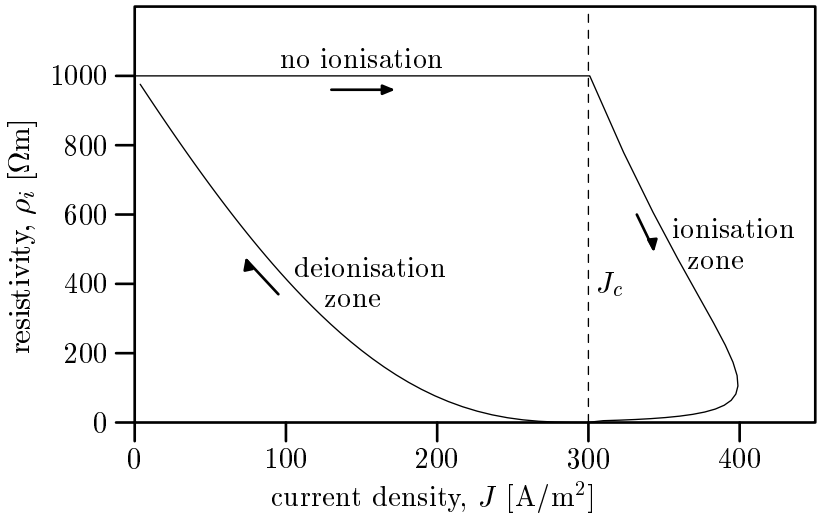

Figure 2.4: Illustrative profile of dynamic resistivity as proposed by Liew & Darveniza (1974). The arrows indicate progression through time.

More recently an extension to the model developed by Liew & Darveniza (1974) was introduced which can account for discrete surface flashovers observed under particular conditions (Wang et al., 2005) – however, several additional empirical parameters are introduced, detracting from the engineering usefulness of the model. In 2006, a very different approach was taken by Sekioka et al. (2006) who observed that the non-linear behaviour of the earth electrode resembles that of a high voltage arc. They proposed an alternative model, based on the widely accepted Cassie-Mayr arc model (CIGRÉ WG 13:01, 1993), that considers the energy balance of the soil ionisation.

When referring to the behaviour or the performance of an earth electrode, it is most convenient to consider the voltage-current relationship which is discussed in the following section.

2.5 Dynamic Impedance of an Earth Electrode

For steady state conditions an earth electrode is described in terms of its resistance to earth. However, under transient conditions, it is important to consider its dynamic impedance as discussed by Nixon & Jandrell (2004*b*). The dynamic impedance of an earth electrode is the ratio of the instantaneous value of earth electrode voltage to the instantaneous value of injected current:

$$Z(t) = \frac{V(t)}{I(t)} \tag{2.5}$$

where

t = time [s]
$Z(t)$ = dynamic impedance of earth electrode at time t [Ω]
$V(t)$ = potential of earth electrode relative to true earth potential at time t [V]
$I(t)$ = current flowing into earth electrode at time t [A]

The challenge introduced in **Chapter 1** is to describe this dynamic impedance for an electrode that is installed in non-homogeneous soil that consists of multiple layers with different resistivities. This suggests an appropriate scope for the thesis.

2.6 Scope of the Thesis

The scope of the thesis is limited to developing a *practical*, yet *accurate*, *simplification* to modelling the *transient behaviour* of a *driven rod earth electrode* in *multi-layer soil*. A driven rod is considered since it is the most basic and most commonly encountered earth electrode system component. The thesis does not address the underlying complex physical processes, nor does it consider large, extended earthing systems as described in IEEE Std 81.2 (1991). The simplified approach described may be applied to models other than that discussed in the thesis, although the limitations inherent in the underlying model would still apply. Note that the thesis is not confined only to the lightning performance of transmission tower earth electrodes, but considers the transient response for general lightning protection studies.

The following chapter defines the problem addressed by the thesis and outlines the approach taken to solve the problem. A suitable earth electrode configuration and the choice of impulse current waveshapes is discussed.

Chapter 3

Approach Taken

The problem addressed by the thesis is defined and the overall approach taken to solve the problem is described. The earth electrode and soil configuration selected for investigation is explained as is the choice of impulse current waveshapes. The contribution made by the thesis is provided.

3.1 Problem Statement

In order to better quantify the behaviour of an earth electrode subjected to a lightning current impulse, it is necessary to understand the commonly encountered scenario of ground with various layers resulting from geological stratification or compacted back-fill. Once this knowledge has been obtained it may then be applied in the design of cost-effective and efficient earthing and lightning protection systems.

The objective of this thesis is to obtain a better understanding of the lightning transient behaviour of an earth electrode in multi-layer soil, and develop a simplified approach to quantifying this behaviour. Specifically, the most common component used in an earthing system, a copper-clad driven rod, is investigated.

3.2 Overall Approach Taken

There were two important components to the approach taken to gain a better understanding of the transient behaviour of a driven rod:

- A dynamic model was developed that could simulate the transient behaviour of the driven rod earth electrode using an electromagnetic transient analysis programme. In this model, the full non-linear effects of ionisation in the surrounding soil were accounted for, and the steady state and the dynamic impedance of the earth electrode could be predicted as a function of applied current magnitude. A method of catering for multiple layers of soil was introduced.
- Measurements were obtained using a large-scale experiment where high current impulses were injected into a single driven rod earth electrode installed in multi-layer soil. The experimental work was used to confirm the results of the model developed.

These two components are discussed in the following sections.

3.2.1 Circuit Model Simulation

A model that predicts the dynamic impedance of a driven rod for a specific impulse current was developed and implemented for the ATP-EMTP, an electromagnetic transient analysis programme. Full details of the model algorithm and its implementation are provided in **Chapter 4**. Additionally, the circuit and the MODELS (Dubé, 1996) source code for the implementation can be found in **Appendix A**.

Parameters used in the model include the geometry of the driven rod, radius r_{rod} and length l_{rod}, the resistivity of the soil, ρ_{soil}, the ionisation time constants, τ_i and τ_d, and the breakdown strength of the soil, E_0. It was proposed that an apparent resistivity value, calculated from the steady state resistance equation and the measured steady state current resistance of the earth electrode, be used for the parameter ρ_{soil}. The model was capable of taking an arbitrary digitised current waveform as an input, enabling its use with real experiment data.

Since this model was a modified version of the dynamic model originally proposed by Liew & Darveniza (1974), it was necessary to establish confidence in the model. This was achieved by comparing the model against an implementation of Liew-Darveniza's model by Anderson (Phillips et al., 2004), and was found to be adequate as discussed in **Appendix B**.

3.2.2 Large-Scale Experiment

Measurements were obtained from a set of large-scale experiments. Due to the challenging nature of the experiment arrangement and the supporting measurement system, thorough calibration and integrity checks were performed before and during testing. For each experiment, all tests were repeated four times to minimise the possibility of erroneous results. All measurements were recorded on a digital storage oscilloscope. These measurements were later processed to remove unwanted noise and to synchronise the voltage and current measurements, since different delays were introduced by the respective measurement devices. Further details about the experiment are provided in **Chapter 5** and specific experiment measurement considerations are included in **Appendix C**.

The large-scale experiment determined the earth electrode geometry, the soil configuration and the impulse current waveshapes that could be studied as summarised in the following sections.

3.2.3 Earth Electrode and Soil Configuration

To verify the model, a driven rod earth electrode configuration was investigated as shown in *Figure 3.1.* Primary characteristics and parameters are summarised on the diagram. The soil consisted of three distinct layers:

- An upper layer of sandy loam.
- A middle portion of clay.
- A lower layer that was below the water table.

The electrode was installed at the test site more than a month before testing commenced and its resistance was monitored during this period to ensure that it remained stable. Precipitation and the depth of the water table were monitored throughout testing. During testing, the steady state electrode resistance was measured using standard test methods (SANS 10199, 2004) to be 48 Ω. This value was confirmed before and after the application of every test impulse current.

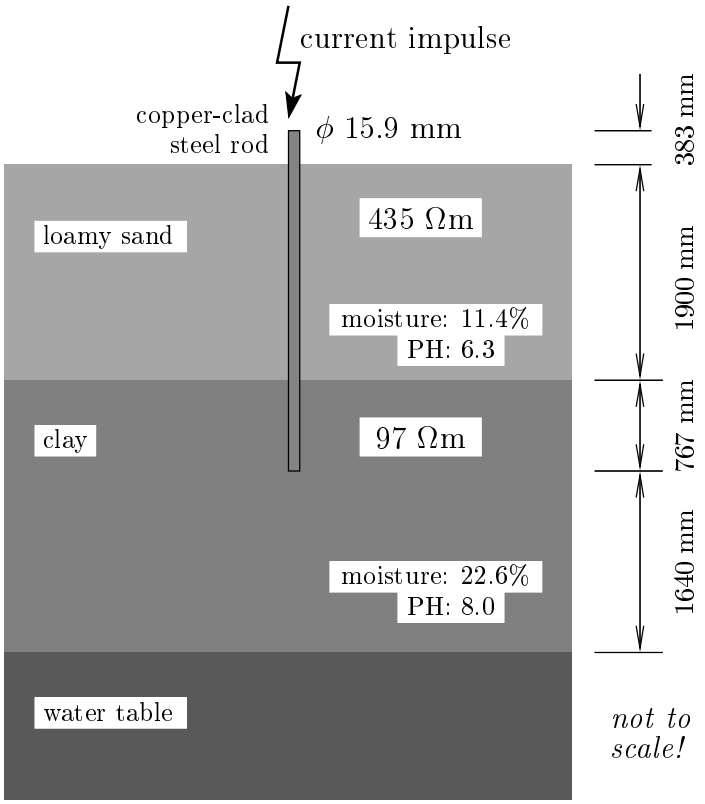

Figure 3.1: Earth electrode and multi-layer soil configuration considered.

3.2.4 Impulse Current Waveshapes

Four different current impulse waveshapes were selected for testing. Since only an outdoor voltage-impulse generator was available at the test site, it was necessary to re-configure the generator to achieve high current impulse outputs. Although the choice of impulse currents was constrained by the capabilities of the available impulse generator, it was still possible to represent a short (1) and a long (2) waveshape, both with low (A) and high (B) peak magnitudes as summarised in *Table 3.1.*

Table 3.1: Impulse current waveshapes (defined as per IEC 60060–1 (1989)).

Shape	**Reference**	**Peak** [kA]	**Waveshape** [μs]
1	I_{1A}	5.2	3.5 / 9.3
	I_{1B}	28.6	3.9 / 9.7
2	I_{2A}	6.7	5.5 / 14.1
	I_{2B}	28.2	5.7 / 13.8

As can be seen in *Table 3.1*, the current waveshapes changed slightly for different current peak magnitudes. This was caused by the dynamic impedance of the electrode presenting a variable impedance to the impulse generator.

Recorded measurements of the actual test currents used are shown in *Figure 3.2*.

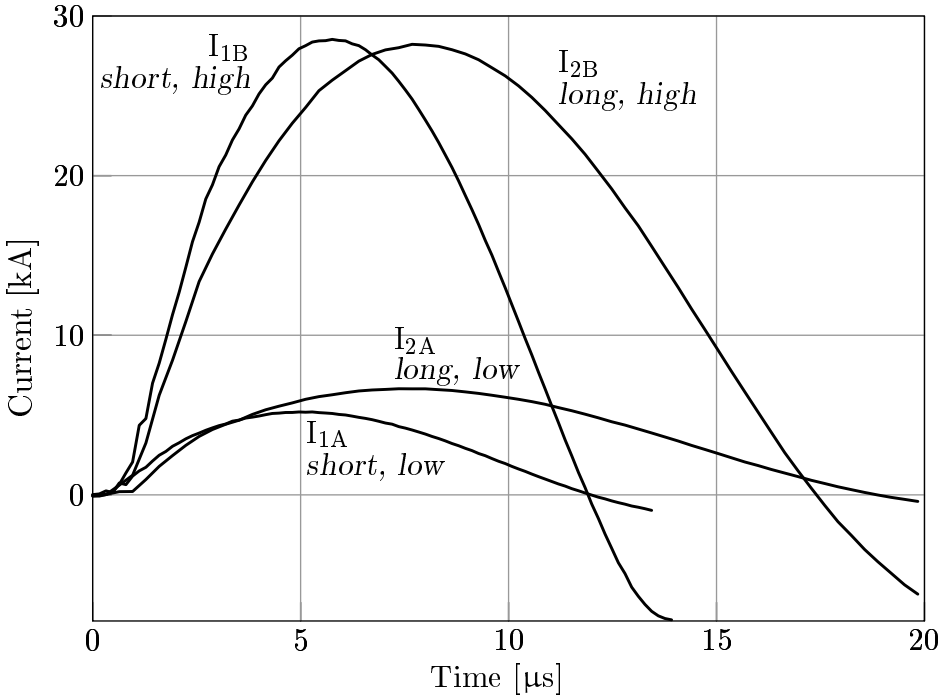

Figure 3.2: Impulse currents used in large-scale experiment and simulations.

Using the measured current impulse waveshapes described the dynamic impedance behaviour of the earth electrode predicted by the circuit simulation model was checked for accuracy against the experiment results.

3.3 Contribution of Thesis

This thesis provides the following unique and valuable contributions to field of earthing and lightning protection:

- An algorithmic representation of a new simplified model used to predict the lightning transient dynamic impedance of a driven rod has been developed. This format enables easy implementation of the model into any chosen simulation environment.

- An implementation of the new model which is suitable for use with ATP-EMTP has been developed. This allows the model to be used in larger, more comprehensive system studies.
- The dynamic impedance predicted by the model has been verified by experimentation.
- It has been shown that for a driven rod earth electrode installed in ground with various layers, rather than having to consider the individual resistivities of all soil layers, acceptable results can be obtained by using only the apparent bulk resistivity value calculated from the steady state resistance equation and the measured steady state current resistance.

In the following chapter the computer model and its derivation for simulating the behaviour of the driven rod earth electrode is introduced. The derivation, the algorithmic representation and subsequent implementation of the model are presented and the choice of parameter values is discussed. In particular, the use of a simplified value of soil resistivity is proposed.

Chapter 4

Circuit Model Simulation

The equivalent circuit model selected to simulate the non-linear behaviour of a driven rod earth electrode in the time-domain is introduced. The derivation, the algorithmic representation and subsequent implementation of the model are presented. The choice of parameter values used in the simulation is discussed, and in particular the use of a simplified value of soil resistivity is proposed.

4.1 Choice of Model

The dynamic model originally proposed by Liew & Darveniza (1974) and subsequently modified and implemented in an electromagnetic transient analysis programme by Nixon (1999) was used to simulate the transient behaviour of the driven rod earth electrode. In this model, the full non-linear effects of ionisation in the surrounding soil are accounted for by introducing two time constants, τ_i and τ_d, which describe the changing resistivity in the surrounding soil under impulse conditions.

Other models and estimation calculations, such as those proposed by Oettlé (1988), Chisholm & Janischewskyj (1989) and CIGRE WG 33:01 (1991) are valuable tools that can be used in transmission line lightning performance calculations, but they are not intended to describe the full time-varying hysteresis observed in practical experiments (Bellaschi et al., 1942; Geri & Veca, 1994; Kosztaluk et al., 1981; Liew & Darveniza, 1974). The full time-domain response of the earth electrode is necessary for this study.

The derivation and implementation of the dynamic model is detailed in the following sections. In essence, the model describes the profile of the dynamically changing

resistivity in the soil surrounding the driven rod earth electrode. This profile consists of the following three intuitive components or zones (Liew & Darveniza, 1974):

1. The zone where there is no ionisation in the soil and the resistivity remains constant.
2. The region in which the critical current density has been exceeded, the resistivity decreases over time to a minimum value with increasing current density.
3. When the critical current density is no longer exceeded in an ionisation zone, the resistivity recovers as the soil de-ionises.

These components can be seen in the resistivity profile curve shown in *Figure 2.4* in **Chapter 2**. In the following section the derivation of the model is discussed.

4.2 Derivation of the Model

Consider a single driven rod of length l_{rod} and radius r_{rod} buried in homogeneous soil with resistivity ρ_{soil} as shown in *Figure 4.1*. Several assumptions must be made in order to derive the model, as explained in the next section.

4.2.1 Initial Assumptions Made

The following initial assumptions are made with respect to the earth electrode shown in *Figure 4.1*:

- The soil surrounding the driven rod is homogeneous and isotropic with resistivity, ρ_{soil}.
- An injected impulse current, I, results in equipotential surfaces that can be approximated by a cylindrical and hemispherical portion, as shown in *Figure 4.1*.
- The current density, J, in the soil at a radial distance, a, from the centre of the driven rod can be approximated by:

$$J = \frac{I}{2\pi(al_{rod} + a^2)}) \tag{4.1}$$

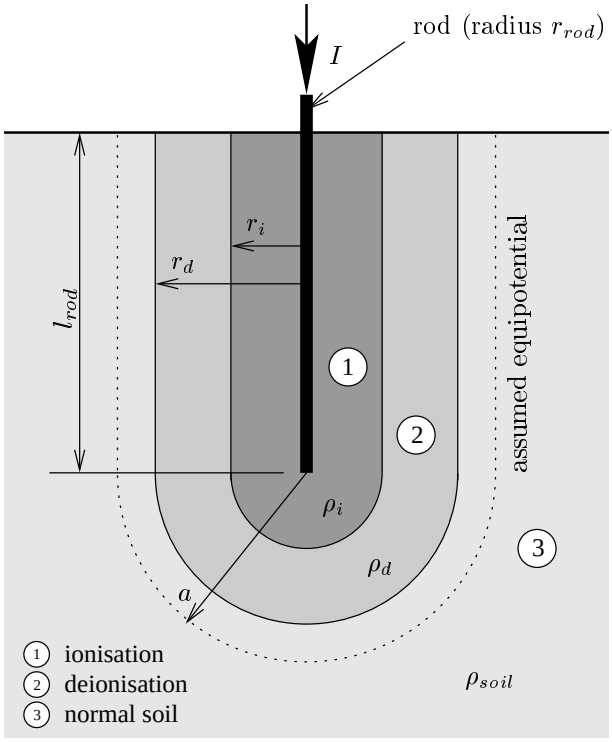

Figure 4.1: Simplified model for the impedance of a single driven rod showing the ionisation and de-ionisation zones envisaged by Liew & Darveniza (1974).

- Breakdown by ionisation occurs in the soil where the current density exceeds a critical value of current density, J_c, given by:

$$J_c = \frac{E_0}{\rho_{soil}} \tag{4.2}$$

- The regions of ionisation and de-ionisation are assumed to be uniform as shown in *Figure 4.1* and the resistivity in these regions is time-varying.

4.2.2 Determining the Effective Resistance of a Driven Rod

Using the assumptions listed in the previous section, Liew & Darveniza (1974) determine the effective resistance of a single driven rod, R_{rod}, by summing elemental shells of resistance, dR, given by:

$$dR = \frac{\rho_a}{2\pi l_{rod}} \left(\frac{1}{r} - \frac{1}{a + l_{rod}} \right) da \tag{4.3}$$

where

ρ_a = resistivity of elemental shell [Ωm]
da = thickness of elemental shell [m]

These elemental shells fall into three distinct regions as shown in *Figure 4.1*:

Region 1 where ionisation is occurring, $J \geq J_c$ and $r_{rod} < a \leq r_i$.
The resistivity of the soil in this region, ρ_i, is given by:

$$\rho_i = \rho_{soil} \exp \frac{-t_i}{\tau_i} \tag{4.4}$$

where

t_i = time since the onset of ionisation [s]
τ_i = ionisation time constant [s]

Region 2 where residual activity exists (de-ionisation), $J < J_c$ and $r_i < a \leq r_d$.
The resistivity of the soil in this region, ρ_d, is given by:

$$\rho_d = \rho_m + (\rho_{soil} - \rho_m)\left(1 - \exp \frac{-t_d}{\tau_d}\right)\left(1 - \frac{J}{J_c}\right) \tag{4.5}$$

where

ρ_m = value of resistivity at onset of de-ionisation given by *Equation (4.4)* [Ωm]
τ_d = de-ionisation time constant [s]
t_d = time measured from the onset of de-ionisation [s]

Region 3 where the resistivity is constant, $J < J_c$ and $a > r_d$.
Resistivity in this region is that of the surrounding soil, ρ_{soil}.

The effective resistance, R_r, can be calculated by summing the resistances of the three regions, and is therefore (Nixon, 1999):

$$R_r = \frac{\rho_i}{2\pi l_{rod}} \ln \frac{r_i(r_{rod} + l_{rod})}{r_{rod}(r_i + l_{rod})} + \frac{\rho_d}{2\pi l_{rod}} \ln \frac{r_d(r_i + l_{rod})}{r_i(r_d + l_{rod})} + \frac{\rho_{soil}}{2\pi l_{rod}} \ln \frac{r_d + l_{rod}}{r_d} \tag{4.6}$$

Note that for the specific case when no ionisation exists, the steady state resistance, as provided in *Equation (4.10)* in **Chapter 3**, is given by:

$$R_{rod} = \frac{\rho_{soil}}{2\pi l_{rod}} \ln \frac{r_{rod} + l_{rod}}{r_{rod}} \tag{4.7}$$

4.3 Algorithm and Implementation

Using the equations and theory discussed in the preceding section, an algorithm for the model that predicts the dynamic resistance of a driven rod for a specific impulse current can be derived. This algorithm is shown in *Figure 4.2* and is discussed in the following section.

Input: t and $|I(t)|$ {from external circuit simulator}
Output: R_{rod} {return to external simulator}

$J_c \Leftarrow \dfrac{E_0}{\rho_{soil}}$ {*Equation (4.2)*}
if $t = 0$ **or** $I(t) = 0$ **then** {help out external transient simulator}{**A**}
  $R_{rod} \Leftarrow \dfrac{\rho_{soil}}{2\pi l_{rod}} \ln \dfrac{r_{rod} + l_{rod}}{r_{rod}}$ {use *Equation (4.7)* as "initial condition"}
else
  $r_i \Leftarrow \dfrac{1}{2}\left(-l_{rod} + \sqrt{l_{rod}^2 + \dfrac{2I(t)}{\pi J_c}}\right)$ {*Equation (4.1)*}
  if $r_i \leq r_{rod}$ **then** {no ionisation occurring}{**B**}
    $r_i \Leftarrow r_{rod}$ {$\therefore$ set to rod radius}
    $\rho_i \Leftarrow 0$ {no ionisation zone}
  else {ionisation has just started or is still occurring}
    if t_i is undefined **then**
      $t_i \Leftarrow t$ {record starting time of ionisation}
    end if
    $\rho_i \Leftarrow \rho_{soil} \exp \dfrac{-t_i}{\tau_i}$ {*Equation (4.4)*}
  end if {end **B**}
  if $r_i > r_d$ **or** r_d is undefined **then** {record maximum extent of ionisation}
    $r_d \Leftarrow r_i$
  end if
  if $r_i < r_d$ **then** {current decreasing $\therefore$ check for de-ionisation zone}{**C**}
    $J_d \Leftarrow \dfrac{I(t)}{2\pi(r_d l_{rod} + r_d^2)}$ {J at de-ionisation boundary - *Equation (4.1)*}
    if $J_d \geq 0.999 J_c$ **then** {flag that J_c has been reached - caters for the case where}
      $F_{Jc} \Leftarrow 1$ {$I(t)$ is decreasing on the wavefront before J_c has been reached}
    end if
    if ρ_m is undefined **and** $t_i > 0$ **and** $F_{Jc} = 1$ **and** $J_d < 0.8 J_c$ **then**
      $\rho_m \Leftarrow \rho_i$ {refer to *Equation (4.5)*}
      $t_d \Leftarrow t$ {record starting time of de-ionisation from below 80% of J_c}
    end if
    if $t_d > 0$ **then** {de-ionisation has commenced}
      $\rho_d \Leftarrow \rho_m + (\rho_{soil} - \rho_m)\left(1 - \exp \dfrac{-t_d}{\tau_d}\right)\left(1 - \dfrac{J}{J_c}\right)$ {*Equation (4.5)*}
    else
      $\rho_d \Leftarrow 0$ {no de-ionisation zone}
    end if
  end if {end **C**}
  $R_i \Leftarrow \dfrac{\rho_i}{2\pi l_{rod}} \ln \left[\dfrac{r_i(r_{rod} + l_{rod})}{r_{rod}(r_i + l_{rod})}\right]$ {R of shells in ionisation zone}
  $R_d \Leftarrow \dfrac{\rho_d}{2\pi l_{rod}} \ln \left[\dfrac{r_d(r_i + l_{rod})}{r_i(r_d + l_{rod})}\right]$ {lumped R of shells in de-ionisation zone}
  $R_n \Leftarrow \dfrac{\rho_{soil}}{2\pi l_{rod}} \ln \left[\dfrac{r_d + l_{rod}}{r_d}\right]$ {R of shells with no ionisation}
  $R_{rod} \Leftarrow R_i + R_d + R_n$ {*Equation (4.6)* derived using *Equation (4.3)*}
end if {end **A**}

Figure 4.2: Algorithm of model used to determine the effective dynamic resistance of driven rod electrode including the effect of soil ionisation. Comments are included in braces {}. Start and end of major conditions marked **X**.

4.3.1 Algorithm Describing the Model

References to equations used from the preceding derivation are included in the algorithm comments shown in *Figure 4.2*. The algorithm takes as inputs the value of time and current magnitude from the external circuit simulation and returns the effective resistance of the driven rod. It consists of the following components:

- Line 2–3 : Start of simulation, return steady state resistance as initial condition to the external circuit simulation.
- Line 5 : Calculate ionisation zone radius which may or may not exist.
- Line 6–8: No ionisation is occurring.
- Line 9–17 : Ionisation has commenced or is continuing. Record starting time of ionisation and keep track of maximum extent of the ionisation zone.
  - Line 13 : Calculate resistivity of ionisation zone (if it exists).
- Line 18–32 : Current density has decreased, therefore there is a possibility that de-ionisation has commenced.
  - Line 20–21 : Ensure that de-ionisation only commences once J_c has been exceeded avoiding false triggers with temporary decreases in current on the wavefront. Due to numerical rounding errors 0.999 is considered close enough to J_c.
  - Line 23–25 : Records starting time of de-ionisation from the point where the current density at the de-ionisation zone radius is 80% of the critical current density (see following discussion). The value of resistivity at the onset of de-ionisation is also recorded.
  - Line 28 : Calculate resistivity of de-ionisation zone (if it exists).
- Line 33 – 36 : Sum the resistances of the three shells to obtain the effective resistance of the driven rod.

In the original model proposed by Liew & Darveniza (1974), since all the elemental shells that form part of the ionisation and de-ionisation region have a different current density for a particular value of current or time, individual calculations would have to be performed for each shell and then summed to obtain the overall resistance. To simplify the algorithm and subsequent coding, the implementation proposed by Nixon (1999) calculates the resistivity of the ionisation and de-ionisation regions as a complete unit using the current density at the outer border of these regions.

To verify this simplification the model was compared against an implementation of Liew-Darveniza's model by Anderson (Phillips et al., 2004) and was found to be adequate as discussed in **Appendix B**. However, the onset time for the de-ionisation zone was found to be incorrect, and it was necessary to modify the implementation such that the start of de-ionisation was recorded once the current density had receded to 80% of the critical current density. This was not a major concern since the critical component of the transient behaviour for lightning protection studies typically occurs before de-ionisation commences (Phillips et al., 2004).

4.3.2 Implementation Considerations

Using the algorithm presented in the preceding section, the model that predicts the dynamic resistance of a driven rod for a specific impulse current was implemented for ATP-EMTP, an electromagnetic transient analysis programme. The advantage of using ATP-EMTP is that it makes it possible to use the model in larger, more comprehensive system studies (Gunther, 1993). Details of the circuit and the MODELS (Dubé, 1996) source code for the implementation can be found in **Appendix A**. Important parameters used in the model include the geometry of the driven rod, r_{rod} and l_{rod}, the resistivity of the soil, ρ_{soil}, the ionisation time constants, τ_i and τ_d, and the breakdown strength of the soil, E_0. In the following section the use of a simplified value of the parameter ρ_{soil} is proposed.

4.4 Simplified Soil Resistivity

Consider *Figure 4.3* which shows a hemispherical earth electrode buried in soil with multiple layers, and *Equations (4.8)* and *(4.9)* from **Chapter 2**.

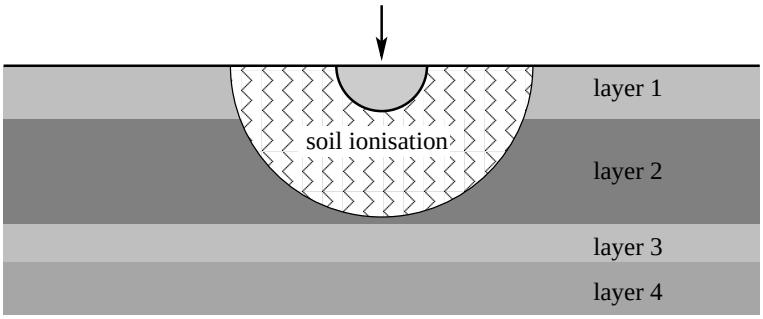

Figure 4.3: Hemispherical earth electrode in multi-layer soil.

$$J = \frac{I}{2\pi r^2} \tag{4.8}$$

$$R_0 = \frac{\rho}{2\pi r_0} \tag{4.9}$$

Since the current density in the soil surrounding the electrode is related to the inverse-square of the distance (*Equation (4.8)*) it can be concluded that when ionisation occurs the resistance of the electrode (*Equation (4.9)*) will be dominated by the resistivity of the ionisation zone. In other words, the effect of layers in the soil will be minimal. Therefore, provided that the model used adequately describes the steady state resistance value of the electrode, complex models of the multiple layers of soil resistivity are not necessary under transient conditions (Nixon et al., 2006).

It is proposed that a single apparent bulk value of resistivity be calculated using the measured low current resistance and the resistance equation – for a hemisphere, *Equation (2.1)*, for a driven rod the equation derived by Liew & Darveniza (1974):

$$R_{rod} = \frac{\rho}{2\pi l_{rod}} \ln \frac{r_{rod} + l_{rod}}{r_{rod}} \tag{4.10}$$

where

R_{rod} = steady state resistance of a driven rod [Ω]
l_{rod} = length of driven rod earth electrode [m]
r_{rod} = radius of driven rod earth electrode [m]

For different earth electrode configurations, *Equation (4.10)* can be replaced by the appropriate equation provided in SANS 10199 (2004).

In practical terms this means that all that is needed for accurate modelling is knowledge of the earth electrode geometry and the measured value of resistance of the earth electrode, obtained using standard techniques (IEEE Std 80, 2000; SANS 10199, 2004). Using these two pieces of information, the apparent resistivity can readily be calculated. This simplification has been used for pragmatic reasons by Sekioka et al. (2006), but no rigorous justification was provided.

In the next section the selection of appropriate values for the other model parameters is discussed.

4.5 Selection of Model Parameters

The selection of the parameters τ_i, τ_d, E_0 and ρ_{soil} for use with the model are considered in this section.

4.5.1 Choice of Ionisation and De-Ionisation Constants

In the absence of more accurate information, the values for the ionisation and de-ionisation time constants, τ_i and τ_d, were taken to be 2 μs and 4.5 μs based on the work performed by Liew & Darveniza (1974).

4.5.2 Choice of Breakdown Strength of Soil

The value of E_0, or the effective breakdown strength of soil, has been the subject of much research (Nixon, 1999). Usually, the value of E_0 was chosen to fit theoretically predicted results to experiment results (Bellaschi et al., 1942; Liew & Darveniza, 1974; Petropoulos, 1948). Oettlé (1988) recommends approximating E_0 as 10 kV/cm due to the inherent complexity of the discharge processes in the soil and suggests that experimental breakdown test results not be used, even if available. Mousa (1994) recommends the value of E_0 should be taken to be 3 kV/cm.

4.5.3 Choice of Soil Resistivity

As discussed in **Section 4.4**, a single apparent bulk value of resistivity was calculated using the measured low current resistance and the resistance equation. Using standard test methods (SANS 10199, 2004) the steady state electrode resistance was measured to be 48.2 Ω. Using *Equation (4.7)* and the dimensions of the driven rod earth electrode that was tested, the apparent bulk value of resistivity was calculated to be 139 Ωm.

4.6 Summary of the Circuit Model

A summary of the key parameter values used in the circuit model is provided in *Table 4.1.*

Table 4.1: Parameter values used in circuit model.

Soil parameters:		
ρ	resistivity [Ωm]	139
E_0	breakdown gradient [kV/m]	300
τ_i	ionisation time constant, [μs]	2.0
τ_d	de-ionisation time constant [μs]	4.5
Electrode parameters:		
r_{rod}	radius of rod [mm]	7.95
l_{rod}	length of rod [mm]	2667

Note that the soil ionisation gradient of 300 kV/m suggested by Liew & Darveniza (1974) and Mousa (1994) was used, contrary to the value of 400 kV/m suggested by CIGRE WG 33:01 (1991). In the absence of known values, the ionisation and de-ionisation time constants suggested by Liew and Darveniza were used. For the scenario considered, ρ was calculated using *Equation (4.7)* and the measured value of R of 48.2 Ω.

The equivalent circuit model used is shown in *Figure 4.4*. The current impulse applied to the circuit was the filtered version of the actual measured current obtained during the experiments. $Z(t)$ in the circuit represents the dynamic resistance produced by the ATP-EMTP model. Using the computer simulation, the predicted voltage $V(t)$ and dynamic impedance $Z(t)$ values were determined.

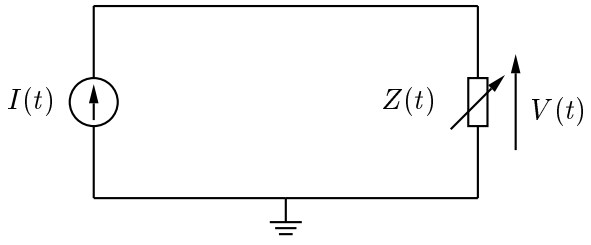

Figure 4.4: Equivalent circuit model implemented in ATP-EMTP.

In the following chapter, the experiment setup used to apply the high current impulses to the earth electrode configuration described in **Chapter 3** is discussed. Details are provided about the overall test site, the impulse generator used, the current and voltage measurement setup and the necessary measurement post-processing.

Chapter 5

Large-Scale Experiment

The selection of a suitable large-scale experiment test site is discussed. Details are provided about the setup used to inject high current impulses into a single driven rod earth electrode in multi-layer soil. Each of the important components involved in the experiment are described, including the impulse generator used, the current and voltage measurement setup and the necessary measurement post-processing employed.

5.1 Selection of Test Site

Very few experiment facilities exist in the world that are capable of injecting large impulse currents representative of actual lightning currents into real earth electrodes. Bellaschi et al. (1942), Liew & Darveniza (1974), Oettlé (1987), Geri et al. (1992), Phillips & Anderson (2002) and Yasuda et al. (2003) are amongst the few that have undertaken full-scale testing. An alternative is to use rocket-triggered lightning as explained by Rakov & Uman (2003), although the peak current magnitudes obtained with this method are often not as high as those of natural lightning and this method is not as repeatable or as controlled as a test facility.

The equipment and the soil configuration at the Electric Power Research Institute (EPRI) Energy Delivery and Utilisation Centre in Lenox, Massachusetts, USA was found to be ideal for obtaining the experiment data required by this thesis. This site was also used to conduct several other significant experiments on earth electrodes as described elsewhere (Nixon et al., 2005; Phillips & Anderson, 2002). A photograph of the test site in which major components are identified is shown in *Figure 5.1* - the key features relevant to this thesis are described in the following sections.

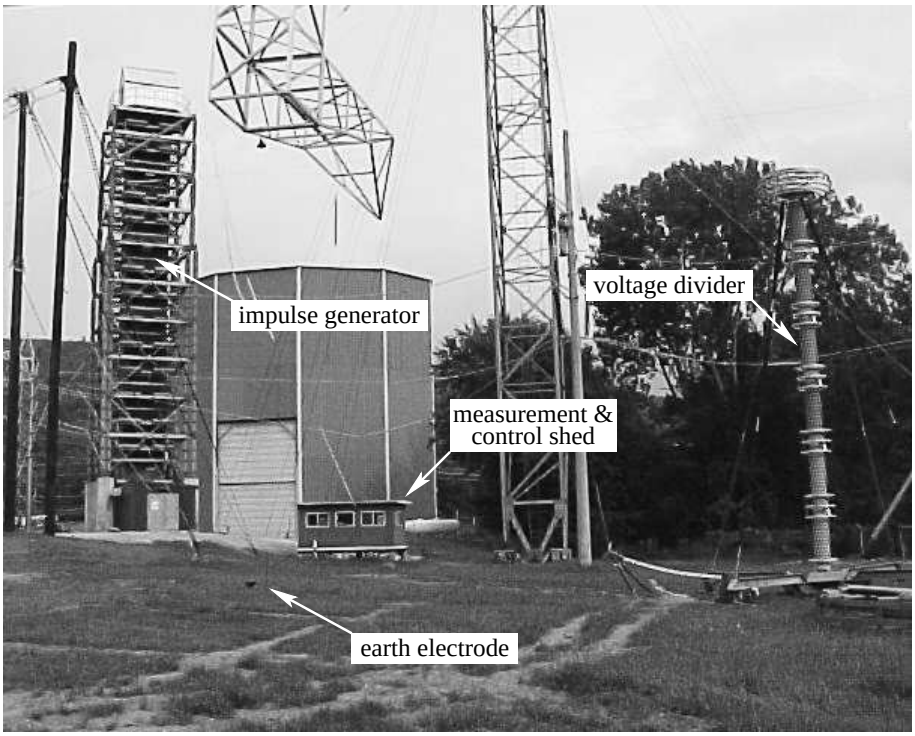

Figure 5.1: Photograph of test site.

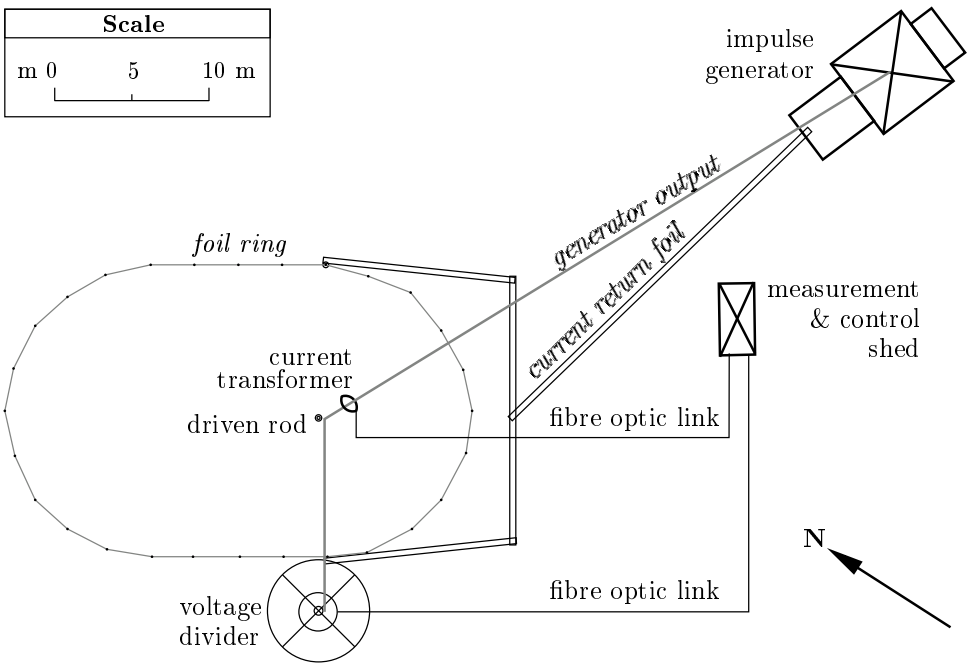

Figure 5.2: Plan view of the test site showing key components of the experiment.

5.2 Overall Test Site

A scale plan view of the overall test site is shown in *Figure 5.2*. An impulse generator was used to inject a current impulse, $I(t)$, into the driven rod. The injected current was measured using a wide bandwidth current transformer and the voltage at the electrode, $V(t)$, was simultaneously measured using an outdoor high voltage impulse divider. Both measurement devices were connected to a digital storage oscilloscope in the measurement and control shed via a fibre optic link system. As explained in more detail in **Section 5.5.2**, attention was paid to minimising the overall inductance of the test configuration as well as to limiting unwanted noise from coupling into the overall measurement system. Special precautions were taken to minimise the voltage induced in the one turn loop formed by the voltage divider, ground and connections to the voltage divider (see also **Appendix C.3**).

5.3 Impulse Generator

The impulse generator used for testing is a 5.6 MV outdoor multi-stage Marx generator with a maximum stored energy of 280 kJ when fully charged. It consists of 28 stages, each with a capacitance of 0.5 μF and capable of being charged to ±100 kV (yielding 200 kV when fired). To achieve the current magnitudes and waveshapes required for the experiment (**Section 3.2.4**), it was necessary to reconfigure the generator by creating series and parallel combinations of the individual stages. The equivalent circuit for the impulse generator is shown in *Figure 5.3* and the parameters in the figure are detailed in *Table 5.1*.

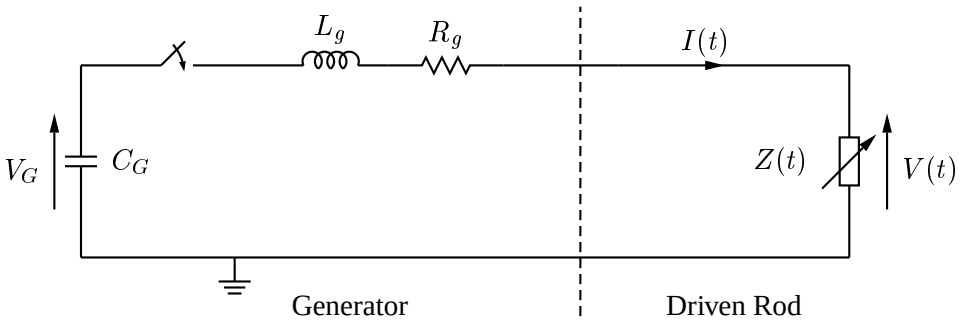

Figure 5.3: Equivalent circuit of the impulse generator and test setup.

Table 5.1: Summary of impulse generator parameters - refer to *Figure 5.3* . Current waveshape 1 and 2 as defined in **Section 3.2.4**.

Parameter	**Details**	**Value**
V_G	Total DC charge voltage on generator (all stages) – variable depending on magnitude of output current required	0 – 1500 kV
L_G	Parasitic inductance of generator	approx. 91 µH
R_G	Parasitic resistance of generator	approx. 0.5 Ω
C_G	Lumped capacitance of generator stages:	
	For waveshape 1 – 7 × 4 stages parallel	0.298 µF
	For waveshape 2 – 9 × 3 stages parallel	0.167 µF

5.4 Test Electrode Configuration

The driven rod was installed within a large elliptical foil ring which consisted of 26 driven rods placed at 3.1 m intervals joined together by a 360 mm wide vertically placed aluminium foil, the top of which was flush with the ground surface (*Figure 5.2*). The outer ring was bonded to the earth of the impulse generator by two aluminium sheet return conductors that provided a low-impedance return path to the generator. This configuration was chosen since it established a well-defined earth reference and a test cell for the driven rod under investigation. The use of flat aluminium sheets and more than one return path helped reduce the overall circuit inductance and resistance, which minimised unnecessary loading of the impulse generator. At all points the outer foil ring was at least 10 m away from the driven rod. The steady state resistance of the rod, measured using the outer foil as a reference, was within 5% of a measurement made using a remote earth reference and it was concluded that 10 m was a sufficient distance for the test configuration.

5.5 Measurement Setup

Due to the large currents and voltages involved it was important to ensure that measurement devices and personnel were galvanically isolated from the test setup.

This was achieved using fibre optic links. The current $I(t)$ and the voltage $V(t)$ were recorded on a digital storage oscilloscope (bandwidth of 250 MHz) via the fibre optic links (bandwidth of 10 MHz). The step wave response of the fibre optic links and oscilloscope was measured prior to testing and confirmed to be within acceptable limits.

5.5.1 Current Measurement

The wide bandwidth current transformer used in the tests was a 301X Pearson Coil with a bandwidth of 2 MHz and a peak impulse current rating of 50 kA. The transmitter of the fibre optic link and the current transformer were coupled together with a steel enclosure in order to reduce unwanted noise coupling into the measurement. The coupled noise was shown to be less than 3% of the measured signal.

5.5.2 Voltage Measurement

The voltage divider used in the tests was a Hipotronics 3 MV mixed capacitive/resistive lightning impulse divider with a division ratio of 3000:1. The divider introduced a delay of 240 ns relative to the current impulse measurement. This delay was due to the propagation time in the 25 m measurement cable and the phase shift caused by the impedance of the divider.

In order to minimise the inductance of the test setup as well as to minimise the flux linkage between the generator–electrode circuit loop and the electrode–measurement circuit loop, the area of both loops was minimised and the loop areas were oriented to one another as close to 90° as possible as shown in *Figure 5.2*. From a practical point of view, this meant that the connecting conductors were run as close to the ground as possible without causing flashovers during testing. It was however necessary to use a 230 kV Cross-linked polyethylene (XLPE) cable between the earth electrode and the voltage divider due to the small clearance distances. The coupled signal on the voltage measurement was estimated to be less than 5% of the measured voltage.

5.6 Measurement Post-Processing

The dynamic impedance, $Z(t)$, of an earth electrode is given by (**Chapter 2**):

$$Z(t) = \frac{V(t)}{I(t)} \tag{5.1}$$

In order to calculate $Z(t)$ using the voltage and current measurements and *Equation (5.1)*, $V(t)$ and $I(t)$ need to be relatively noise-free. It was therefore necessary to filter the measurements. A low-pass fifth-order Chebyshev type-II filter (Stearns & David, 1988) with 40 dB attenuation in the stop band and cutoff frequency 10 MHz was applied to the signals. Additionally, Fourier analysis of the measured signals revealed an unusual peak at around 940 kHz (attributed to inductive ringing in the test setup). This was filtered out using a band-stop second-order Chebyshev type-II filter (Stearns & David, 1988). This matter is discussed in more detail in **Appendix C** where the source of the noise is explained, and both the raw and the filtered measurements are presented.

Post-processing was also necessary to synchronise the $V(t)$ and $I(t)$ measurements, since the voltage divider introduced a 240 ns delay relative to the current measurement. This delay was due to the long length of cable integral to the functioning of the divider.

At the beginning of the current impulse, where the current and voltages are low, there is typically too much noise to reasonably calculate the dynamic impedance. Hence, graphs involving calculated curves only start after 1 µs. Additionally, measurements after the zero-crossing of the current impulse are meaningless in the context of the thesis, therefore only measurements up to 10 µs were considered for current waveshape 1 and up to 15 µs for current waveshape 2.

In the following chapter the simulation and experiment results are compared and discussed. It is shown that there is strong agreement between the simulated and experiment values supporting the simplification introduced by the thesis.

Chapter 6

Comparison of Results and Discussion

The results are compared and discussed in this chapter. There is strong agreement between the simulated and experiment values supporting the simplified approach introduced by the thesis. Some thoughts on modelling and the validity simplified value of soil resistivity used are presented.

6.1 Comparison of Results

The results from circuit model simulation discussed in **Chapter 4** and the large-scale experiment discussed in **Chapter 5** are compared in *Table 6.1*.

Table 6.1: Summary of experiment and simulation results. Simulation results are shown in parenthesis.

	Current $I(t)$			**Voltage** $V(t)$		**Impedance** $Z(t)$	
#	**Ref.**	**Peak** [kA]	**Shape** [μs]	**Ref.**	**Peak** [kV]	**Ref.**	**Min.** [Ω]
1	I_{1A}	5.2	3.5 / 9.3	V_{1A}	151 (146)	Z_{1A}	26.2 (25.7)
	I_{1B}	28.6	3.9 / 9.7	V_{1B}	492 (514)	Z_{1B}	13.5 (15.2)
2	I_{2A}	6.7	5.5 / 14.1	V_{2A}	166 (161)	Z_{2A}	22.7 (23.3)
	I_{2B}	28.2	5.7 / 13.8	V_{2B}	447 (438)	Z_{2B}	12.6 (13.8)

6.1.1 Summary

As can be seen in *Table 6.1* the minimum transient impedance of a driven rod earth electrode is considerably lower than its steady state resistance. This is true even for relatively low values of impulse current, where the reduction is around 50% for both current waveshapes. For high current values the reduction is as much as 80% of the steady state value. The results support the dynamic model used in the thesis since the reduction is slightly more marked for the longer current waveshape which is consistent with the concept of an ionisation time constant.

The following sections present the results in more detail. For each current waveshape two figures are shown: the first contains the current and voltage curves, the second contains the current and dynamic impedance curves. As discussed in **Chapter 2** the dynamic impedance is calculated using:

$$Z(t) = \frac{V(t)}{I(t)} \tag{6.1}$$

6.1.2 Current Waveshape 1

The results for current waveshape 1 are shown in *Figure 6.1.* The curves in the figure are labelled consistent with the referencing system shown in *Table 6.1.* Although the experiment results have been filtered as discussed in **Appendix C** the inductive ringing is still partly present. Since the simulated results are created using the actual experiment current this ringing appears in the simulated voltage waveshapes as well. The noise resulting from the firing of the impulse generator is also evident within the first 1 μs of the current and voltage waveshapes. As a result the dynamic impedance during this time is meaningless and has therefore been omitted from the curves.

6.1.3 Current Waveshape 2

The results for current waveshape 2 are shown in *Figure 6.2.* Again the curves in the figure are labelled consistent with the referencing system shown in *Table 6.1*, and the initial part of dynamic impedance curves is not shown due to the noise created by the firing of the impulse generator. Note that the simulated and experiment curve for V_{2B} differ - the sag before the current peak for the experiment measurement was due to a partial failure in the firing mechanism of the impulse generator where the high current magnitude caused a coiled spring mechanism to fail.

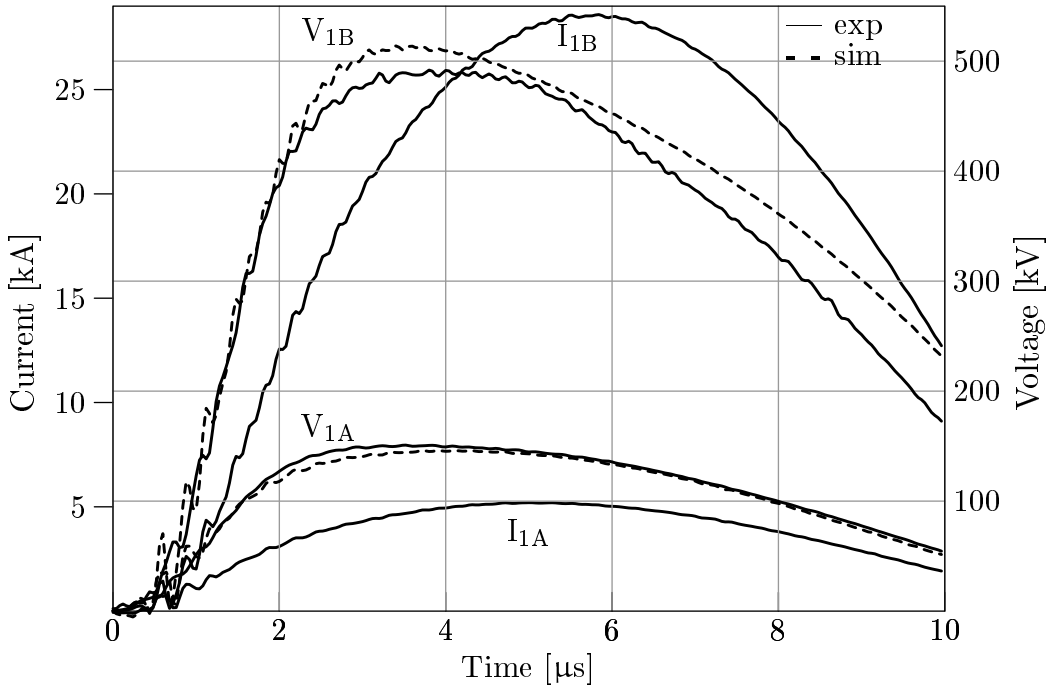

(a) Current and voltage.

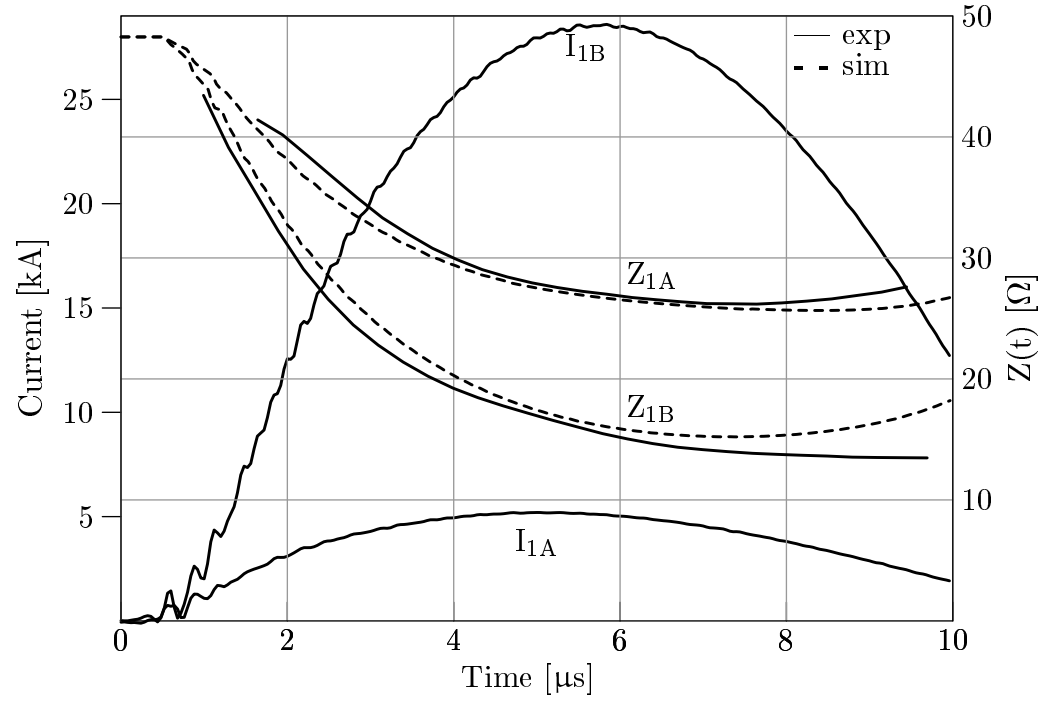

(b) Current and dynamic impedance.

Figure 6.1: Comparison of experiment (solid line) and simulated (dashed line) voltage and dynamic resistance values for current waveshape 1 – 4/10 µs, 5 kA and 29 kA. Multiple axes are used to plot current, voltage and impedance.

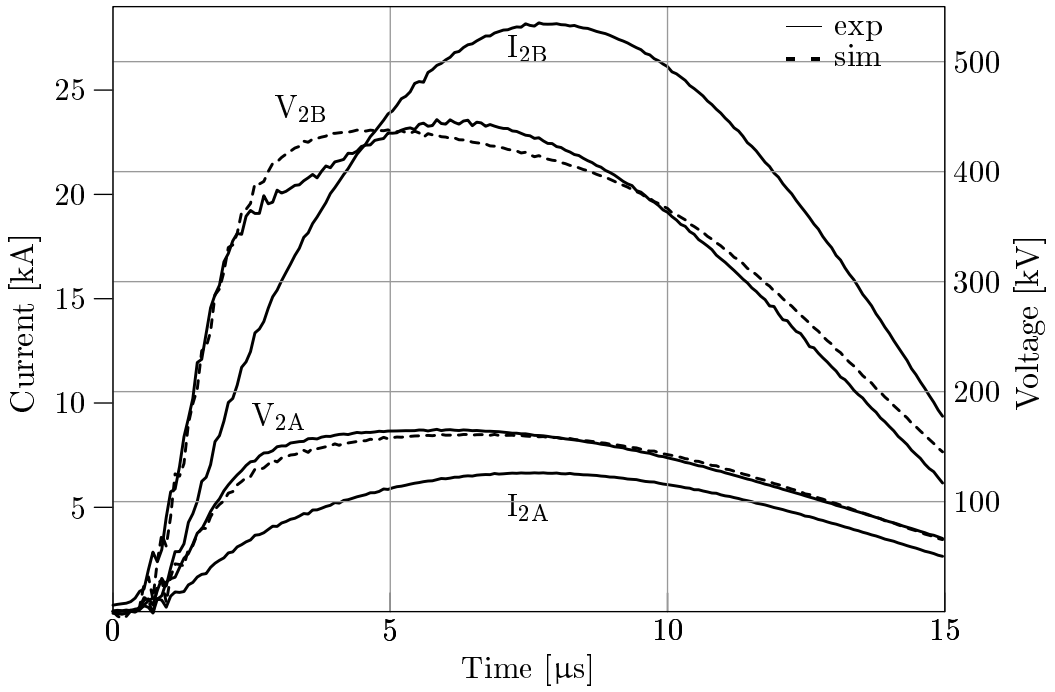

(a) Current and voltage.

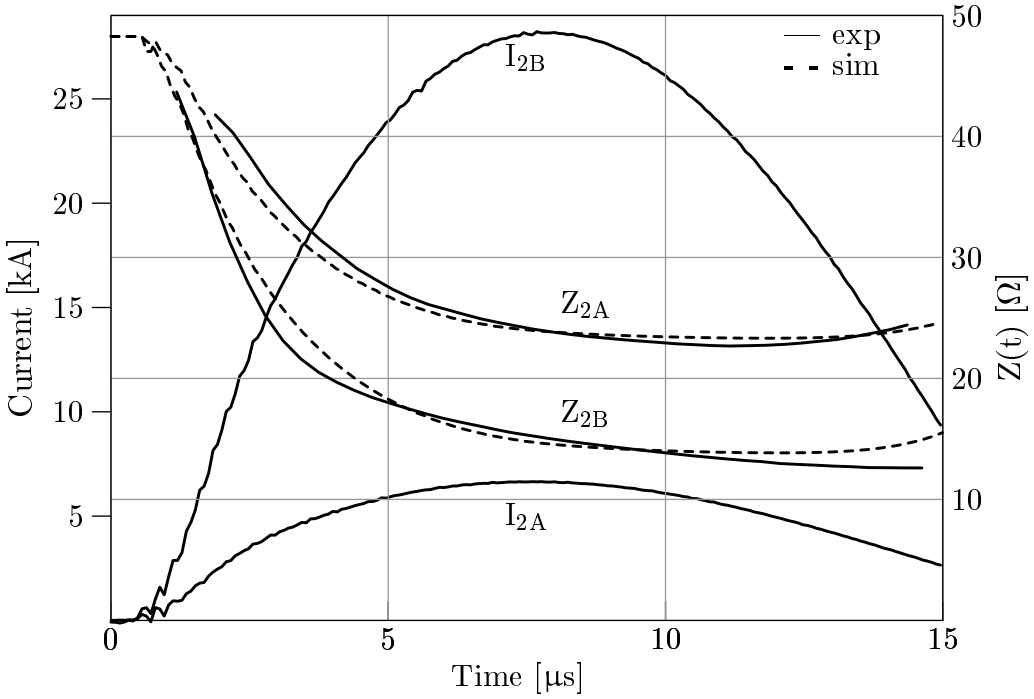

(b) Current and dynamic impedance.

Figure 6.2: Comparison of experiment (solid line) and simulated (dashed line) voltage and dynamic resistance values for current waveshape 2 – 6/14 µs, 7 kA and 29 kA. Multiple axes are used to plot current, voltage and impedance. Note that the timescale is different to *Figure 6.1.*

6.2 Discussion

There is strong agreement between the experiment and simulated values as can be seen in *Table 6.1* and *Figures 6.1* and *6.2*. The only minor discrepancy occurs towards the end of the large magnitude current impulses where the simulated impedance increases more than the experiment impedance. However, this phenomenon can also be observed in the paper by Liew & Darveniza (1974) and has been further addressed in recent work (Sekioka et al., 2006).

To explain why the simplification introduced by the thesis works, consider the simulated resistivity profile at a radius of 200 mm from the centre of the rod as shown in *Figure 6.3*. The profile was generated using current I_{1B} applied to the circuit model discussed in **Chapter 4**. The times of key points are indicated on the curve. It is clear that the resistivity of the soil in the immediate vicinity of the rod rapidly reaches very low values in the dynamic model. Consequently, the effect of any local or remote differences in resistivity due to soil layering is minimised, since the soil ionisation around the electrode dominates the impedance of the driven rod.

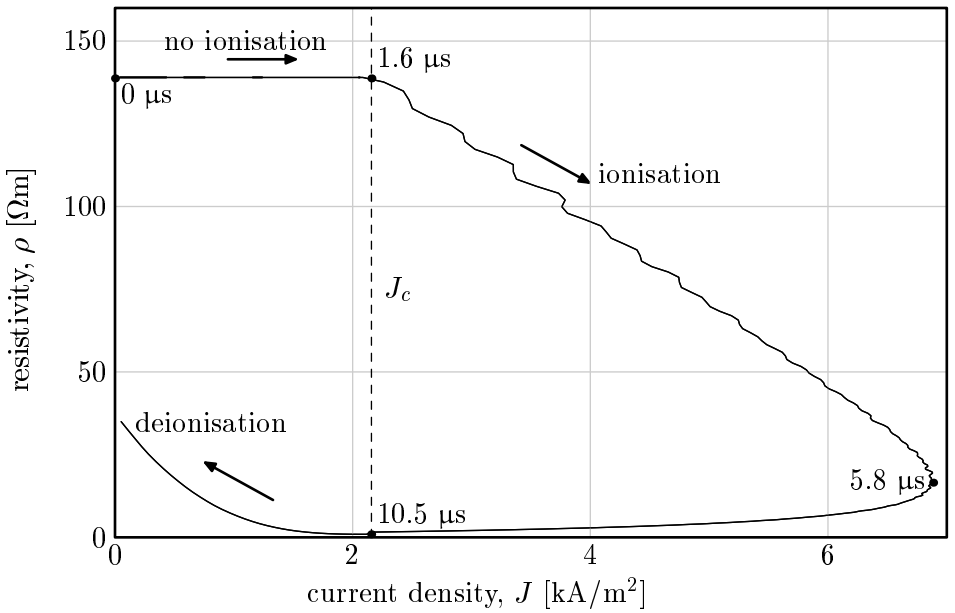

Figure 6.3: Resistivity profile at a radius of 200 mm from the centre of the driven rod generated by the dynamic impedance model. The time value at specific points of the profile are shown.

6.3 Validity of the Simplification

It is important to note that although measurable physical parameters are included in the simulation model, the model makes no attempt to be an accurate reflection of the actual physical processes that occur. The model is considered sufficient in that it can predict the behaviour of an earth electrode subjected to a current impulse suitable for engineering studies. Although some research has been published on the physical processes (Erler & Snowden, 1983; Leadon et al., 1983; Oettlé, 1987; Snowden & Erler, 1983), the processes involved are not yet fully understood, primarily because it is difficult to visually observe exactly what occurs under the surface of the ground.

In fact, little physical evidence exists to support the concept of a uniform ionisation zone, and observations such as streamers occurring across the surface of the earth and the formation of fulgurites in sand (Rakov & Uman, 2003) suggest that breakdown typically occurs in discrete channels. Petropoulos (1948) proposed that the breakdown activity may look more like that shown in *Figure 6.4a*. For a driven rod the activity may look like that shown in *Figure 6.4b*. The length of these channels rarely exceeds 10 m (Phillips et al., 2004).

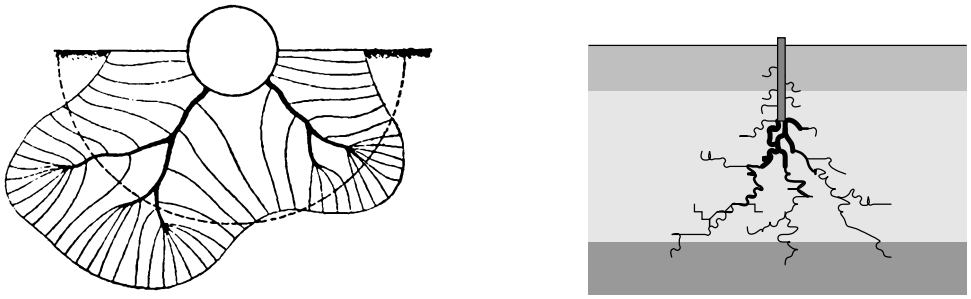

(a) Petropoulos (1948). *(b)* Driven rod.

Figure 6.4: Discrete breakdown channels around an earth electrode.

Nonetheless the simplification introduced in this thesis will still be valid for a discrete channel breakdown model, since it can be argued that the resistance of the breakdown channel is likely to dominate the transient behaviour of the earth electrode, and not the surrounding soil.

In the following chapter, the findings of the thesis are summarised and areas for further research are identified.

Chapter 7

Conclusion and Recommendations

7.1 Conclusion

It has been shown that for a driven rod earth electrode installed in ground with various layers, rather than having to consider the individual resistivities of all soil layers, acceptable results can be obtained by using only the apparent bulk resistivity value calculated from the steady state resistance equation and the measured steady state current resistance. This represents a unique and valuable contribution to the field of earthing and lightning protection since it is a useful simplification to modelling the transient behaviour of an electrode in commonly occurring soil conditions. The simplification has been verified using large-scale experiment results and a simulation model for impulse currents of up to 30 kA magnitude.

7.2 Recommendations for Further Research

The work discussed in this thesis provides a solid base upon which further research in several areas can be performed:

- Additional experiment data obtained through testing a range of earth electrode geometries under differing soil conditions would provide further verification of the simplified approach introduced in the thesis. However, these experiments will require considerable time and resourcing.
- More importantly, the physical processes that occur in the soil surrounding an earth electrode subjected to a lightning current impulse are still not fully

understood. Further research needs to focus on developing a method of visually recording the breakdown processes involved to improve our understanding in this area. The work performed by Hayashi (1967), where X-ray film under an earth electrode was used, should be revisited and explored further using modern image processing techniques.

- Measuring the absolute voltage developed on an earth electrode necessary for obtaining the dynamic impedance behaviour remains a challenge, and the novel method proposed by Nixon et al. (2005) must be investigated further. The recent development of a cost-effective field mill and a re-usable rocket suitable for triggered lightning experiments by Grant & Nixon (2006); Grant et al. (2006) promise to be useful tools in testing this method, and answering many other earthing and lightning protection research questions.

- The design by Nixon & Jandrell (2004*a*) of a modular and scalable measurement system for measuring the dynamic impedance of cellular base station earth electrodes must be fully implemented to obtain invaluable information about earth electrode performance under natural lightning conditions.

Appendix A

ATP-EMTP Source Code

This appendix contains the following ATP-EMTP source code:

- The MODELS implementation of the dynamic resistance described in **Chapter 4**.
- An overview of the ATP-EMTP circuit and the corresponding main data case file used to generate the simulation results in **Chapter 6**.

A.1 Introduction

For convenience, line numbers are provided on the left of the source code listings. Keywords are shown in **bold** and any comments are shown in *italics*. For further information on the keywords, syntax and structure of ATP-EMTP refer to Meyer & Liu (1982) and Dubé (1996).

A.2 Modified Liew-Darveniza Dynamic Model

The MODELS implementation of the modified Liew-Darveniza dynamic resistance of a driven rod, as described in **Chapter 4**, is provided on the following pages. Refer to *Figure 4.2* (Page 21) for the algorithmic representation of this code.

```
C ------------------------------------------------------------------------
C NIXONROD.MOD  18 Jan 2005
C
C         - Modified Liew-Darveniza model for concentrated electrodes
C
C Notes: Considers ionisation and deionisation zones as one complete
C        shell and not several sub-shells - good enough approximation
C ------------------------------------------------------------------------

MODEL nixonrod
------------------------------------------------------------------------
COMMENT
  Model derived from paper "Dynamic model of impulse characteristics
  of concentrated earths" by Liew and Darveniza, Proc. IEE,
  Vol. 121, No. 2, Feb 1974.

  Important parameters of the model are:
    rodr  -  radius of driven rod
    rodl  -  depth of driven rod
    E0    -  critical sparkover voltage gradient, "gc"
    taui  -  ionisation time constant
    taud  -  deionisation time constant
    rho0  -  low-current value of resistivity
  Inputs and output:
    Iin   -  current into earth resistance node
    timex -  "present" moment in time (needed for ionisn time consts)
    RES   -  resistance of earth rod
ENDCOMMENT
------------------------------------------------------------------------
 INPUT                      -- inputs to model
  Iin
  timex
 OUTPUT                     -- output of model
  RES
 DATA                       -- set some defaults
  rodr  {dflt: 0.008}
  rodl  {dflt: 1.8}
  E0    {dflt: 1000000}         -- E0 in V/m
  taui  {dflt: 2e-6}
  taud  {dflt: 4.5e-6}
  rho0  {dflt: 1000}
 VAR Iabs, RES, ionr, deionr, idens, idensc, rhoion, rhodeion
     RESi, RESd, RESn, tdeiononset, tiononset, rhom, gotidensc
 INIT
  deionr := 0               -- max. radius of ionisn ("rcm")
  ionr := 0                 -- radius that describes ionisn zone
  idensc := E0 / rho0       -- critical current density
  idens := 0                -- current density for deionisn zone
  rhom := -1                -- need to wait till later to find this out
  tiononset := -1           -- onset time of ionisation (-1=no ion yet)
  tdeiononset := -1         -- onset time of deionisation (-1 no deion)
  gotidensc := -1           -- have reached idensc at some point
  rhoion := 0               -- resistivity of ionisn zone (0 initially)
  rhodeion := 0             -- same for deionisn zone (0 initially)
 ENDINIT
```

```
55
    EXEC
     Iabs := ABS(Iin)        -- make sure we have *magnitude* of current

     IF Iabs = 0 OR timex = 0 THEN -- NB low current conditions apply
60                                 -- for I=0, t=0 - helps ATP out
      RES := rho0/(2*PI*rodl) * LN( (rodr+rodl)/rodr )
     ELSE                      -- now we must look at where ionisation is
      -- ionisation critical radius (soln of current density calc)
      ionr := (-rodl + SQRT(rodl*rodl + 2*Iabs/(E0/rho0*pi))) / 2
65    IF ionr < rodr THEN  -- basically no ionisation - set to rodr
       ionr := rodr
     ENDIF

   -- Consider ionisation region, if applicable
70    IF ionr <= rodr THEN -- if no ionisn, resistivity of region=0
       rhoion := 0
     ELSE
      IF tiononset = -1 THEN  -- got start of ionisn, make a note
       tiononset := timex      -- save present time
75    ENDIF
                    -- resisty in region given by eqn 8 in Liew paper
      rhoion  := rho0 * EXP(-(timex-tiononset)/taui)
     ENDIF

80   IF ionr > deionr THEN  -- ionisn zone must have extended, thus
      deionr := ionr         -- make a note of this new max radius
     ENDIF                    -- ultimately this is "rcm" boundary

   -- Consider deionisation region, if applicable
85   IF ionr < deionr THEN  -- got deionisation zone if this is true
                                -- current density calculation
      idens := Iabs / (2*PI*deionr*rodl + 2*PI*deionr*deionr)

                 -- some numerical rounding means we must look for .999
90    IF idens >= 0.999*idensc THEN  -- reached critical current density
       gotidensc := 1             -- needed to mark start of deion
      ENDIF
                              -- if deionisation not already happening
      -- cater for noisy current waveform and the fact that not all
95    -- shells are considered
      IF rhom = -1 AND tiononset <> -1 AND
                       gotidensc <> -1 AND idens < 0.8*idensc THEN
       rhom := rhoion   -- record this parameter ('rhoi' in Liew paper)
       tdeiononset := timex  -- "t" is defined from deionisn onset
100   ENDIF
                              -- need to calc deionisn rho if started
      IF tdeiononset <> -1 THEN      -- now we have deionisation
                         -- next, region where ionisn was present, but
       rhodeion := rhom + (rho0-rhom) *   -- Jc no longer exceeded
105         (1 - EXP(-(timex-tdeiononset)/taud)) * (1 - idens/idensc)**2
      ENDIF
     ELSE                      -- otherwise, ensure no deionisation zone
      rhodeion := 0
     ENDIF
```

```
110
   -- Now find the constituent resistances of the zones
      RESi := rhoion/(2*PI*rodl)
      RESi := RESi*( LN( deionr*(rodr+rodl) / (rodr*(ionr+rodl) ) ) )

115   -- deionisation (should strictly consider sub-shells, but
      RESd := rhodeion/(2*PI*rodl)      -- lumping as one is good enough
      RESd := RESd*( LN( deionr*(ionr+rodl) / (ionr*(deionr+rodl) ) ) )

      -- no ionisation here
120   RESn := rho0/(2*PI*rodl) * LN( (deionr+rodl)/deionr )

   -- Effective resistance is sum of the other components
      RES := RESi + RESd + RESn

125  ENDIF
   ENDEXEC
   ENDMODEL
```

A.3 ATP-EMTP circuit detail

Figure A.1 provides an overview of the ATP-EMTP circuit used to generate the simulation results which will assist in understanding the main data case file.

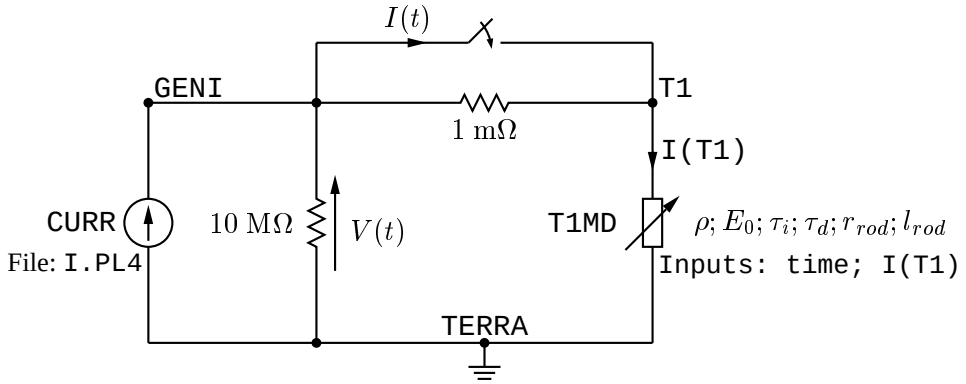

Figure A.1: Detail of the ATP-EMTP circuit used to generate the simulation results. Node names (`GENI`,`T1`,`TERRA`) and selected details are provided to facilitate understanding of the main data case file shown in the following section.

A.4 Main Data Case File

The main data case file for the ATP-EMTP simulation is listed below. The correct column alignment of characters in an ATP-EMTP data case file is essential, and has therefore been retained in the listing.

```
C ------------------------------------------------------------------------------
C  SIMULATE.DAT                          2005-01-19
C
C     Use measured current waveshape from large scale experiments and
C     dynamic resistance model to simulate voltage and resistance.
C ------------------------------------------------------------------------------
BEGIN NEW DATA CASE
C ---  template for next card.   MULPPF  LUNPPF  L63TYP
POSTPROCESS PLOT FILE                  1       63       3
C Modify "i.pl4" in the following line for different experiment currents
$OPEN, UNIT=63   FILE=[]i.pl4     !       { Expected to be C-like (L4BYTE = 1)
C deltat     tmax     xopt     copt   epsiln   tolmat   tstart
   8.E-9   25.E-6        0        0
C Use the following for shorter duration current waveshapes
C   4.E-9   15.E-6        0        0
C  print  points  connec     s-s  minmax     vary    again     plot
       1       1       1       1       1                        2
C NB - must have plot set to 2 otherwise source pl4 gets removed
C ==============================================================================
MODELS

INPUT    currk {PL4(1)}
         time {ATP(t)}
OUTPUT   geni

-- I/O for models
------------------------------------------------------------------- Input/Output
INPUT
-- driven rod
         it1 { i(t1) }
OUTPUT
--driven rod
         t1md
------------------------------------------------------------------- Model definitions:
MODEL lcursrc                -- experiment current "source"
 VAR
  curr
 INPUT
  timex, currt
 OUTPUT
  curr
 EXEC
  curr := currt
 ENDEXEC
ENDMODEL
                             -- include dynamic resistance model definition
$INCLUDE nixonrod.mod
```

```
------------------------------------------------------------------ Model instances:
-- The current source
USE
  lcursrc AS geni
    INPUT timex := time
          currt := currk
    OUTPUT geni := curr
ENDUSE
-- The driven rod : Note that the defaults in NIXONROD are:
--       rodr=0.008, rodl=1.8, E0=1000000, tau1=2e6, tau2=4.5e-6, roe0=?
USE
  nixonrod AS t1md
    DATA
      rho0 := 139
      rodl := 2.667
      rodr := 0.0159/2
      E0 := 300000
    INPUT  Iin := it1
           timex := time
    OUTPUT t1md := res
ENDUSE
------------------------------------------------------- Printed/plotted variables:
RECORD t1md.res AS t1md

ENDMODELS
C ============================================================================
C                                  Branch cards
C driven rods
C NODE 1NODE 2TACS  RES          { T91 is Resistance (using models)
91T1           TACS  T1MD
C Make sure current source appears "connected" to injection point
C NODE ANODE BNODE CNODE D     R      L      C
  GENI  T1                  0.001
C Avoid numerical oscillations and record measurement
  GENI                      10.E6                                            2
BLANK card ending branch cards
C ============================================================================
C                                  Switch cards
C Switch in the lightning current
  GENI  T1                                              MEASURING            1
BLANK card ending switch cards
C ============================================================================
C                                  Source cards
C       IV              0=volt -1=curr
60GENI  -1
BLANK card ending source cards
C ============================================================================
C                                  Output variables
C NODE1 NODE2 NODE3 NODE4 NODE5 NODE6 NODE7 NODE8 NODE9 NODE10NODE11NODE12NODE13
BLANK card ending output variable requests
C ============================================================================
BLANK card ending plot cards
C ============================================================================
BEGIN NEW DATA CASE
BLANK card ending session
```

Appendix B

Modified Dynamic Impedance Model

The key modification introduced to the Liew-Darveniza model in **Chapter 4** is summarised. Using current waveshapes and parameter values similar to those used in body of the thesis the modified model is compared against an alternative implementation. It is concluded that the modified model adequately describes the dynamic behaviour of a driven rod earth electrode.

B.1 Modified Liew-Darveniza Model

The simulation results obtained using the model described in **Chapter 4** compare favourably with the experiment results as shown in **Chapter 6**. However, this model is a significantly modified version of the one originally proposed by Liew & Darveniza (1974). In the Liew-Darveniza model multiple shells of resistance are considered, each with thickness d, and each in their own state of ionisation and de-ionisation. The modified version simplifies this by considering only three major zones, effectively lumping multiple shells together, as detailed in the algorithmic representation of the model (*Figure 4.2* on Page 21). This key difference is summarised in *Figure B.1* where the three major zones are indicated.

To investigate the impact of this modification the behaviour predicted by the modified model is compared to that predicted by an implementation of Liew-Darveniza's model by Anderson (Phillips et al., 2004, Appendix B). In the following sections the current waveshapes and parameter values used for the comparison are discussed, and the findings of the investigation are summarised.

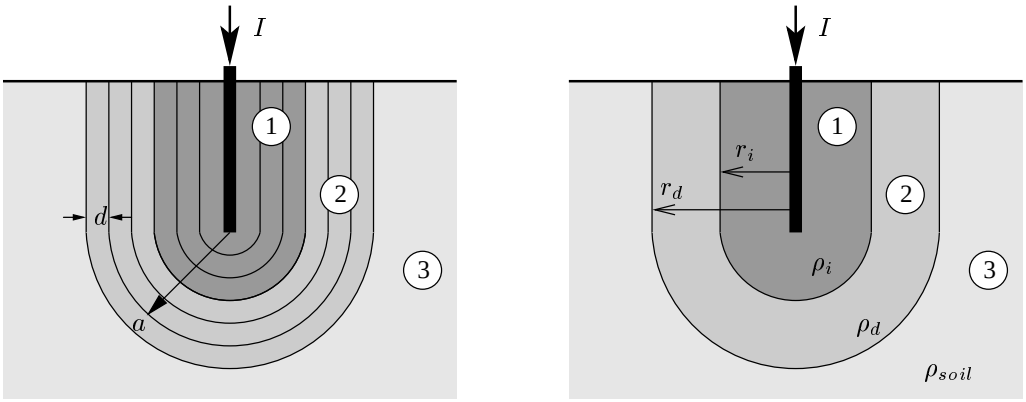

(a) Liew-Darveniza *(b)* Modified model by Nixon

Figure B.1: Illustrating the key difference between the modified and original Liew-Darveniza model. Three major zones exist: (1) ionisation, (2) deionisation and (3) no activity.

B.2 Current Waveshapes Used for Comparison

Current waveshapes similar to those used in the large-scale testing, summarised in *Table B.1*, were used when comparing the two models. The tail-time of the current waveshapes was set to 35 μs since the Anderson model enforced this lower limit, being more representative of a realistic lightning current tail-time (Anderson & Eriksson, 1980). In the following section the parameter values used in the comparative simulations are provided.

Table B.1: Current impulse waveshapes used for model comparison.

Shape	**Reference**	**Peak** [kA]	**Waveshape** [μs]
1	I_{1A}	5	4 / 35
	I_{1B}	30	4 / 35
2	I_{2A}	5	6 / 35
	I_{2B}	30	6 / 35

B.3 Parameter Values

The parameter values used as inputs to both models are summarised in *Table B.2*. The parameters are as similar as possible to those used in the body of the thesis (discussed in detail in **Chapter 4**). Most importantly a bulk apparent resistivity of the multi-layer soil is used. The results are presented in the next section.

Table B.2: Parameter values used in models.

Soil parameters:		
ρ	resistivity [Ωm]	140
E_0	breakdown gradient [kV/m]	300
τ_i	ionisation time constant, [μs]	2.0
τ_d	de-ionisation time constant [μs]	4.5
Electrode parameters:		
r_{rod}	radius of rod [mm]	8
l_{rod}	length of rod [mm]	2700

B.4 Results

The results of the comparative study are summarised in *Table B.3*. The steady state resistance value, minimum dynamic value and percentage reduction are provided for each current waveshape. As can be seen the minimum dynamic impedance is similar for both current waveshapes since the extended tail-time results in more ionisation and hence more reduction in resistance for both waveshapes. Note that the steady state value for the Anderson model is 6% higher since the Sunde (1949) equation was used rather than the Liew & Darveniza (1974) equation. However, there is good agreement between the two models for the percentage reduction in impedance and both models produce similar dynamic impedance curves as shown in *Figure B.2*.

Table B.3: Comparison between Nixon's modified Liew-Darveniza model and Anderson's Liew-Darveniza model. Values for Anderson's model are shown in parenthesis. Note: S.-S.⇒Steady State; Redn⇒Reduction.

	Current $I(t)$			**Impedance** $Z(t)$			
#	**Ref.**	**Peak** [kA]	**Shape** [μs]	**Ref.**	**S.-S.** [Ω]	**Min.** [Ω]	**% Redn**
1	I_{1A}	5	4 / 35	Z_{1A}	48.1 (51.2)	25.4 (28.2)	53% (55%)
	I_{1B}	30	4 / 35	Z_{1B}		13.5 (16.6)	28% (32%)
2	I_{2A}	5	6 / 35	Z_{2A}	48.1 (51.2)	25.4 (28.3)	53% (55%)
	I_{2B}	30	6/ 35	Z_{2B}		13.5 (16.7)	28% (33%)

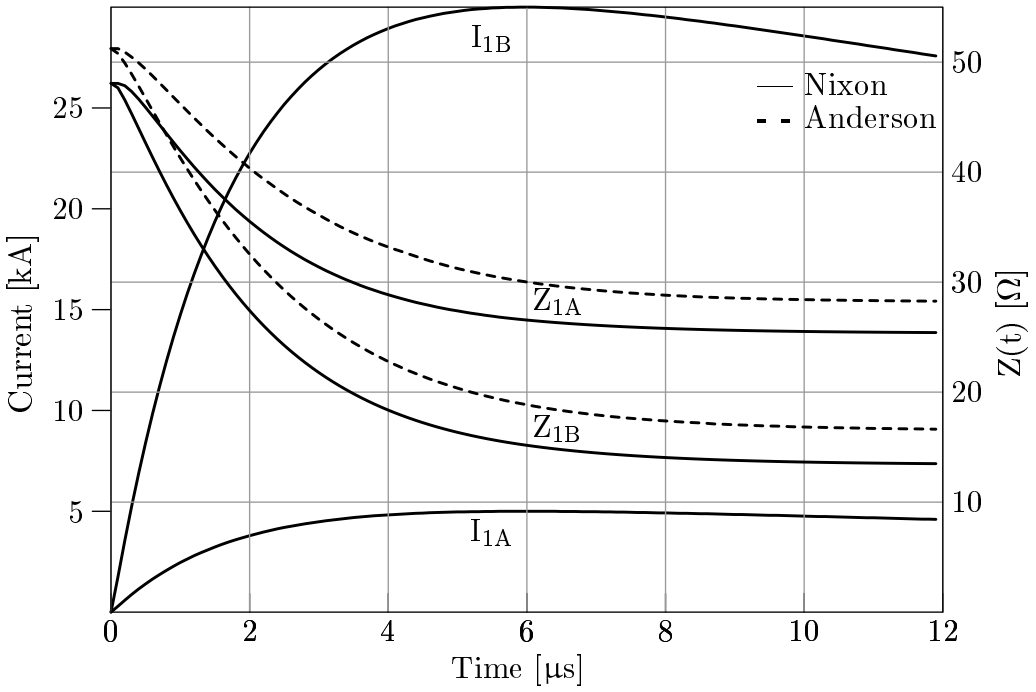

(a) Current waveshape 1 – 4/35 μs.

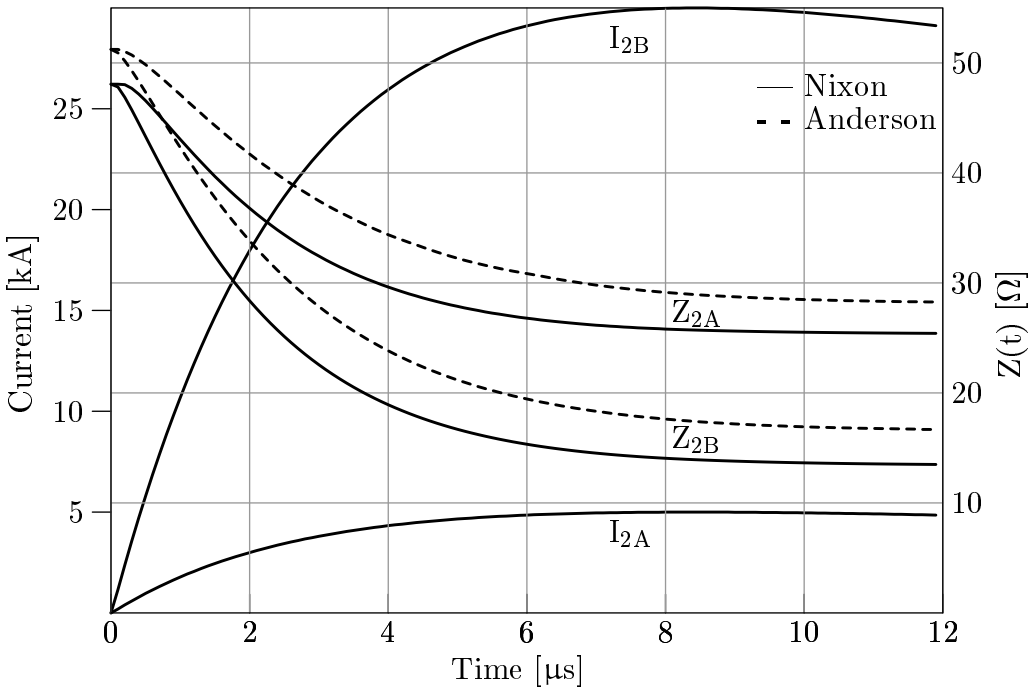

(b) Current waveshape 2 – 6/35 μs.

Figure B.2: Comparison between Nixon's modified Liew-Darveniza model (solid line) and Anderson's Liew-Darveniza model (dashed line) dynamic resistance behaviour. Multiple axes are used to plot current and and impedance.

B.5 Conclusion

Results obtained using the modified version of the model originally proposed by Liew & Darveniza (1974) agree with the experiment data as well as an alternative implementation by Anderson (Phillips et al., 2004, Appendix B). Although there is a small difference (6%) in the predicted steady state value the trend of the non-linear behaviour is very similar between the two models. It is concluded that the modified model adequately describes the non-linear dynamic behaviour of a driven rod earth electrode.

Appendix C

Measurement Considerations

The measurement challenges encountered in the experiment are discussed. The inadvertent resonance in the setup is characterised and its source is explained. Details are provided on the filter used to remove the unwanted noise. The raw unfiltered and final filtered experiment data is presented.

C.1 Measurement Challenges

Significant measurement challenges were introduced by the physical extent of the experiment setup, the substantial electromagnetic noise generated, and the high magnitudes of di/dt involved. Special attention was therefore given to preventing unwanted noise coupling into the measurements through the use of good bonding and shielding practises, as can be seen in *Figure C.1.*

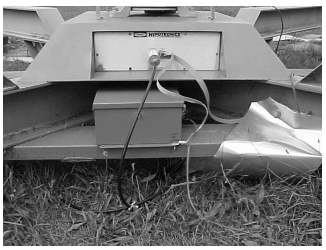

(a) Low voltage arm of high voltage divider and fibre optic transmitter.

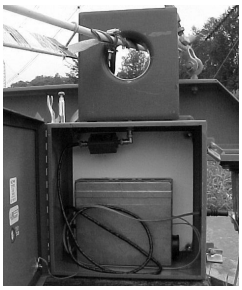

(b) Current transformer and fibre optic transmitter.

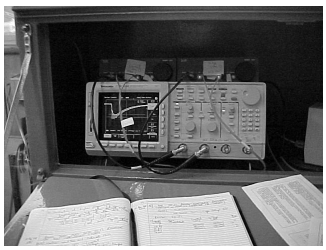

(c) Digital storage oscilloscope and fibre optic receiver enclosed in shielded box (closed during firing).

Figure C.1: Photographs of measurement equipment. All sensitive components were shielded by using ferromagnetic enclosures and thorough bonding.

Despite these efforts, initial stages of testing revealed that an inadvertent resonance had been introduced due to the components and geometry of the experiment setup. This resonance manifested itself as an inductive ringing and was particularly evident on the front of the voltage measurements for high current impulses. Given the limitations of the equipment and the physical geometry involved there was little that could be done to avoid this ringing, and it was necessary to filter the measurements to remove the noise. The following sections characterise this inductive ringing, explain its source and its removal, and show the raw unfiltered measurements from which the data used in the body of the thesis is derived.

C.2 Frequency Analysis of Measurement with Noise

To investigate the inductive ringing observed in the measurements the earth electrode under test was "removed" from the circuit by directly connecting the top of the electrode to the surrounding elliptical foil ring electrode (described in **Section 5.4**) using a wide flat piece of aluminium foil. A low magnitude current impulse, −3 kA, was then applied to the setup and the measurement made by the voltage divider was recorded. In theory the measurement should approximately describe $V = Ldi/dt$ since only the volt-drop across the 10 m long flat piece of foil is being measured. However, as can be seen in *Figure C.2a*, the inductive ringing is still evident. The discrete Fourier transform of this measurement, shown in *Figure C.2b*, reveals a significant peak near 1 MHz.

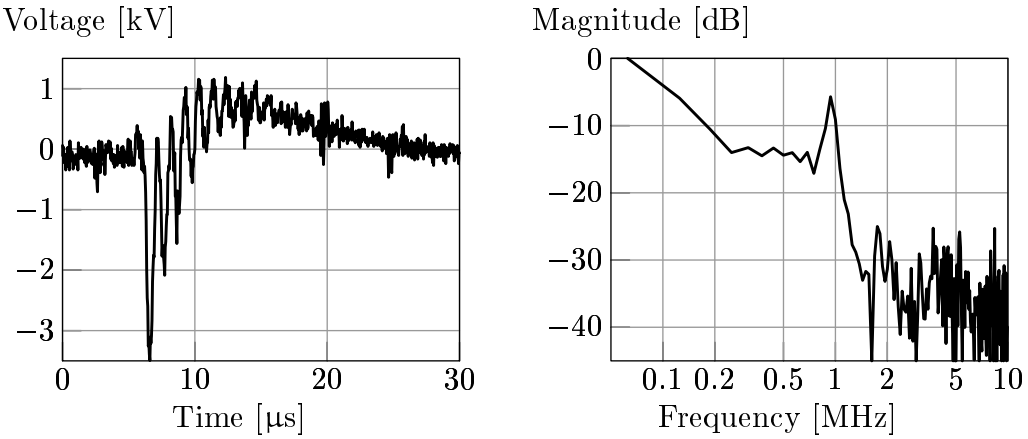

(a) Voltage measured across aluminium foil.

(b) Discrete Fourier transform of signal.

Figure C.2: Measurement containing inductive ringing obtained by shorting out the earth electrode under test.

To understand the source of this unwanted noise it is necessary to analyse the measurement circuit involved, and this is done in the following section.

C.3 Analysis of Voltage Measurement System

A photograph illustrating the test arrangement described in the previous section is shown in *Figure C.3*. Details of the connections between various points of the setup are provided in a list following the figure.

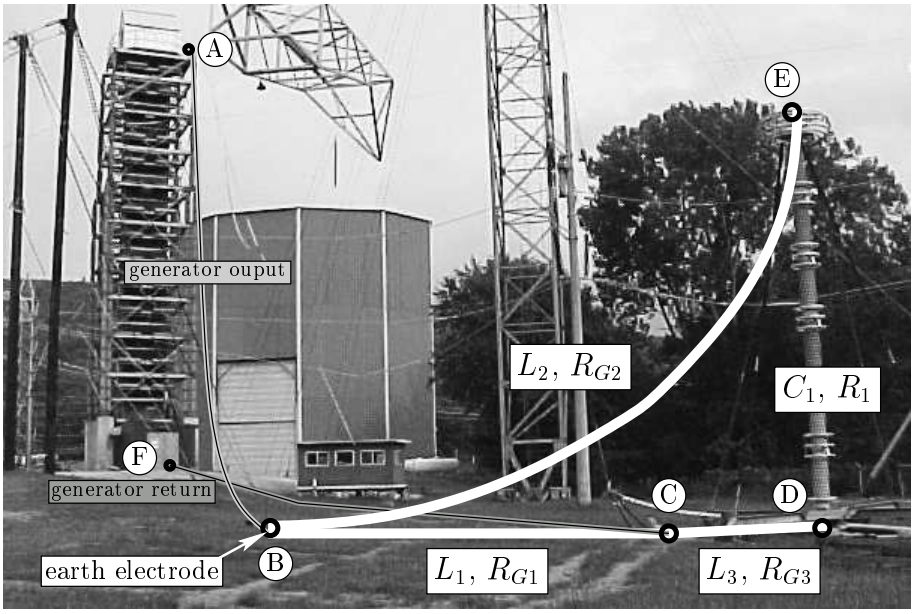

Figure C.3: Photograph of high voltage measurement circuit. Key points are shown (**A. . . F**) as well as circuit parameters introduced in *Figure C.4*.

Point (A) to (B): the output of the generator is connected to the driven rod earth electrode. This connection was shaped in a sweeping arc to minimise the loop area **(A-B-F)**, hence minimising the flux linkage to loop **(B-D-E)**, thereby reducing unwanted noise from coupling into the voltage measurement.

Point (B) to (C): this connection was not present during normal testing and was only introduced to investigate the ringing noise. It shorts out the earth electrode by making a direct connection to the outer elliptical ring electrode. The self-inductance and resistance of this connection are denoted L_1 and R_{G1}.

Point (C) to (D): this is the bond between the high voltage divider earth and the overall experiment earth with self-inductance and resistance L_3 and R_{G3}.

Point (B) to (E): the driven rod earth electrode is connected to the high voltage input of the divider. Again this connection was shaped in a sweeping arc to minimise the loop area **(B-D-E)**, hence minimising unwanted noise coupling into the measurement from loop **(A-B-F)**. The self-inductance and resistance of this connection are denoted L_2 and R_{G2}.

Point (C) to (F): this connection ensures that there is a defined earth return path to the impulse generator. Not shown in the figure is a second additional connection from the outer ring electrode to the generator earth (refer to *Figure 5.2*).

Point (D) to (E): this is not a connection, but indicates the high voltage arm of the mixed capacitive/resistive lightning impulse divider. The capacitance and resistance of the high voltage arm denoted C_1 and R_1 respectively.

A simplified equivalent circuit of this setup is shown in *Figure C.4*. In the circuit, a current consisting of a range of frequency components is injected through the foil (L_1, R_{G1}). The injected current develops a voltage, V_m, which is the objective of the measurement. The foil is joined to the high voltage impulse divider with non-zero impedances (L_2, R_{G2} and L_3, R_{G3}). As a simplification the effect of mutual impedances are ignored in the model. The voltage divider consists of a high voltage arm (C_1, R_1), a low voltage arm (C_2) and a measurement cable (R_2, C_3). The input impedance of the fibre optic measurement transmitter is represented by R_3.

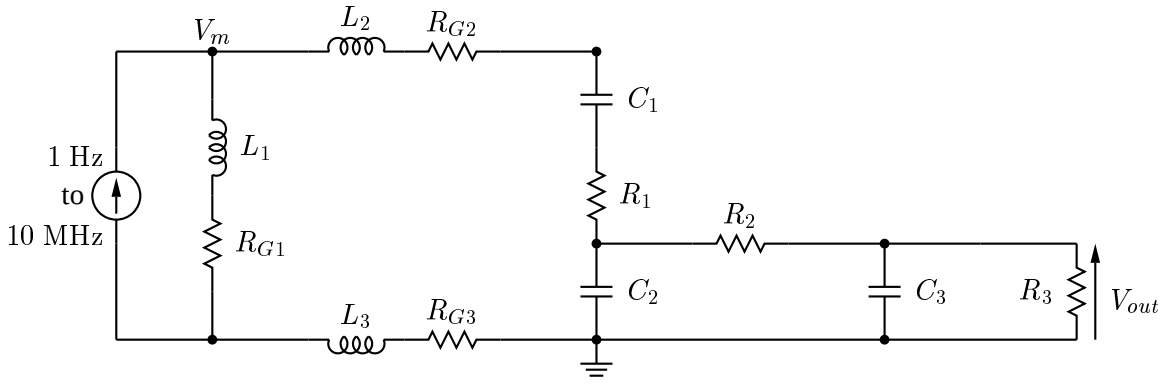

Figure C.4: High voltage impulse divider measurement circuit. Component details and values are provided in *Table C.1.*

A summary of the components and their values is provided in *Table C.1.* The impedances of the measurement connections were approximated by assuming a per unit length self inductance of 1.2 μH/m (Grover, 1962) and resistance of 1 Ω/km. The voltage divider measurement cable was 25 m in length and had a characteristic impedance of 75 Ω and per unit length capacitance of 65.6 pF.

Table C.1: Summary of components in equivalent circuit of high voltage impulse divider measurement circuit - refer to *Figure C.4* .

Parameter	Details	Value
L_1, R_{G1}	Self inductance and resistance of **(B-C)**	12 μH, 0.01 Ω
L_2, R_{G2}	Self inductance and resistance of **(B-E)**	18 μH, 0.015 Ω
L_3, R_{G3}	Self inductance and resistance of **(C-D)**	4.8 μH, 0.004 Ω
C_1	Capacitance of high voltage arm of divider	500 pF
R_1	Resistance of high voltage arm of divider	150 Ω
C_2	Capacitance of low voltage arm of divider	750 nF
R_2	Characteristic impedance of the measurement cable connected to the divider	75 Ω
C_3	Lumped capacitance of measurement cable	1.64 nF
R_3	Input impedance of fibre optic system	10 MΩ

The measurement setup was analysed by performing a SPICE simulation (Pederson et al., 1989) of the equivalent circuit shown in *Figure C.4*. A fixed current magnitude was injected into the circuit over a range of frequencies to obtain the frequency response of the system. The results of the analysis are shown in *Figure C.5*. Clearly evident is the peak that occurs around 1 MHz. The simulation was repeated with the foil (L_1, R_{G1}) replaced by a 50 Ω resistor representative of the steady state resistance of the driven rod. The same resonance peak was observed, although it was attenuated relative to the previous simulation. It was concluded that the unwanted inductive ringing was a result of the measurement circuit configuration and that it would be necessary to filter the measurements. The filter that was used to remove the ringing is summarised in the following section.

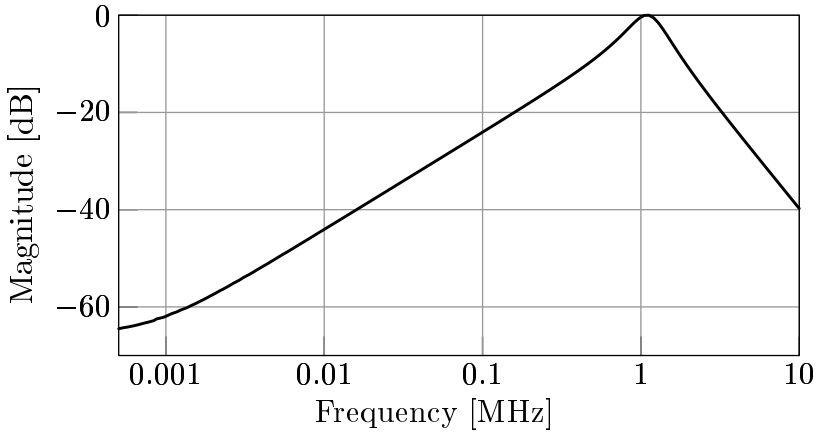

Figure C.5: Normalised frequency response of voltage measurement system.

C.4 Filter Details

The unwanted ringing was removed by post-processing the raw measurements using a digital band-stop second-order Chebyshev type-II filter (Stearns & David, 1988). The filter had 40 dB attenuation in the stop and edges at 800 kHz and 1100 kHz. The frequency response of the implemented filter is shown in *Figure C.6*. The filter was applied to both voltage and current measurements to prevent the phase shift introduced by the filter from affecting the calculation of the dynamic impedance of the electrode, $Z(t) = V(t)/I(t)$. In the following section the raw unfiltered and final filtered measurements are presented.

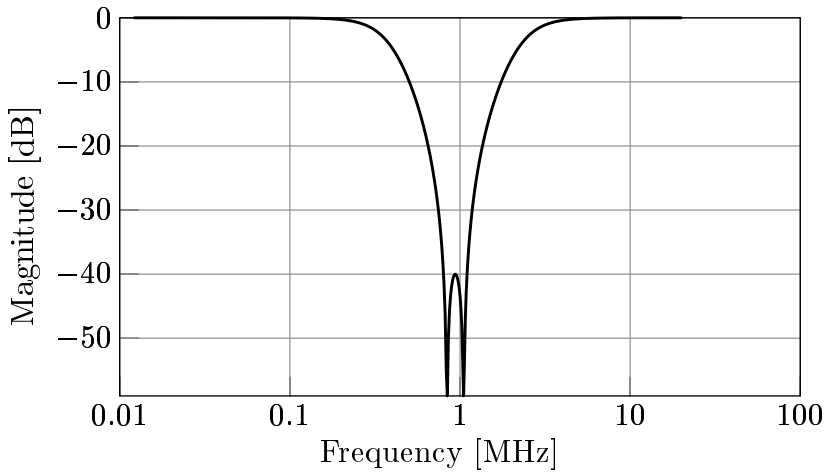

Figure C.6: Frequency response of filter used to remove unwanted signal.

C.5 Raw and Filtered Experiment Data

The raw unfiltered and final filtered experiment data is shown in *Figures C.7* and *C.8*. Note that additional post-processing has been applied to the final filtered data, including the adjustment for the delay between the current and voltage measurement systems as well as the application of a 10 MHz low pass filter. This additional post-processing is explained in more detail in **Section 5.6**.

As can be seen in *Figures C.7a* and *C.8a* the filtered experiment voltage and current measurements no longer contain the unwanted inductive ringing, enabling better calculation of the dynamic impedance data as shown in *Figures C.7b* and *C.8b*.

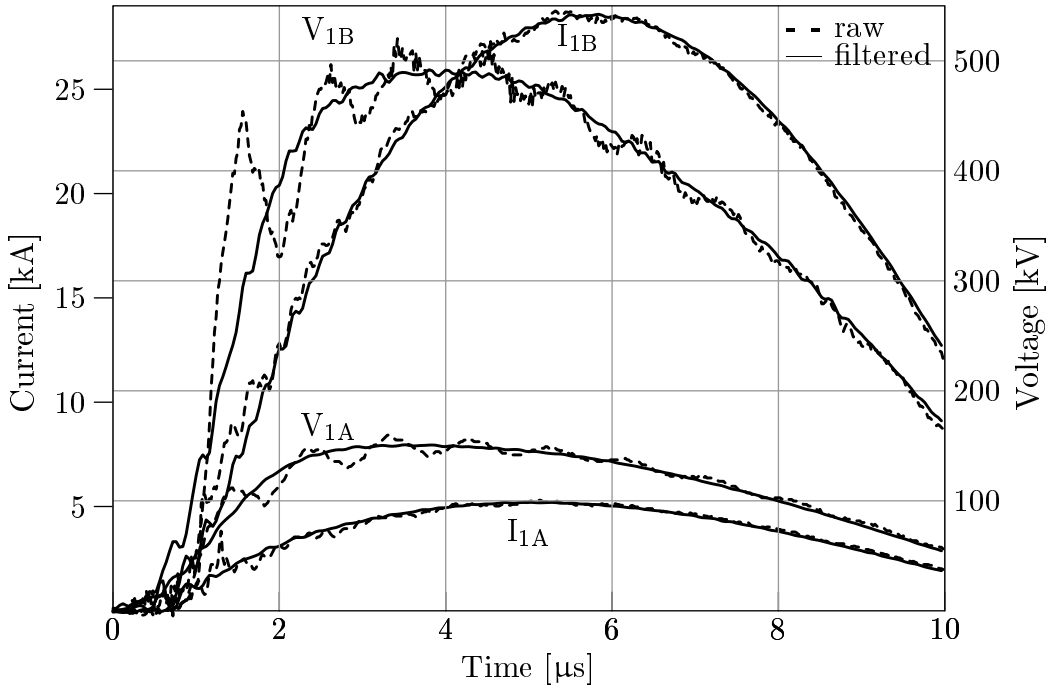

(a) Measured current and voltage.

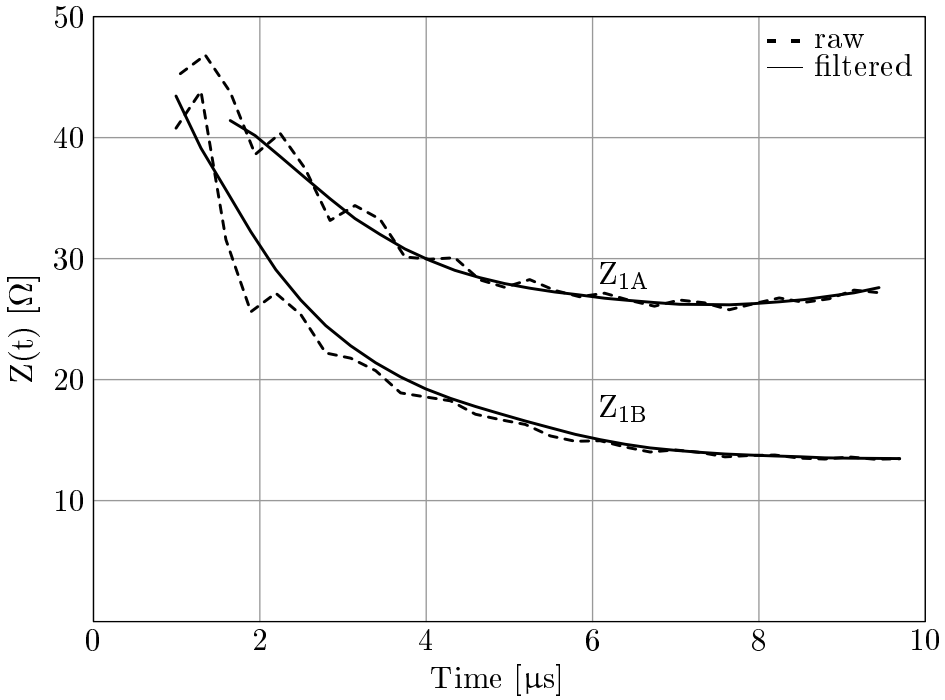

(b) Calculated dynamic impedance.

Figure C.7: Raw (dashed line) and filtered (solid line) experiment data for current waveshape 1 – 4/10 µs, 5 kA and 29 kA.

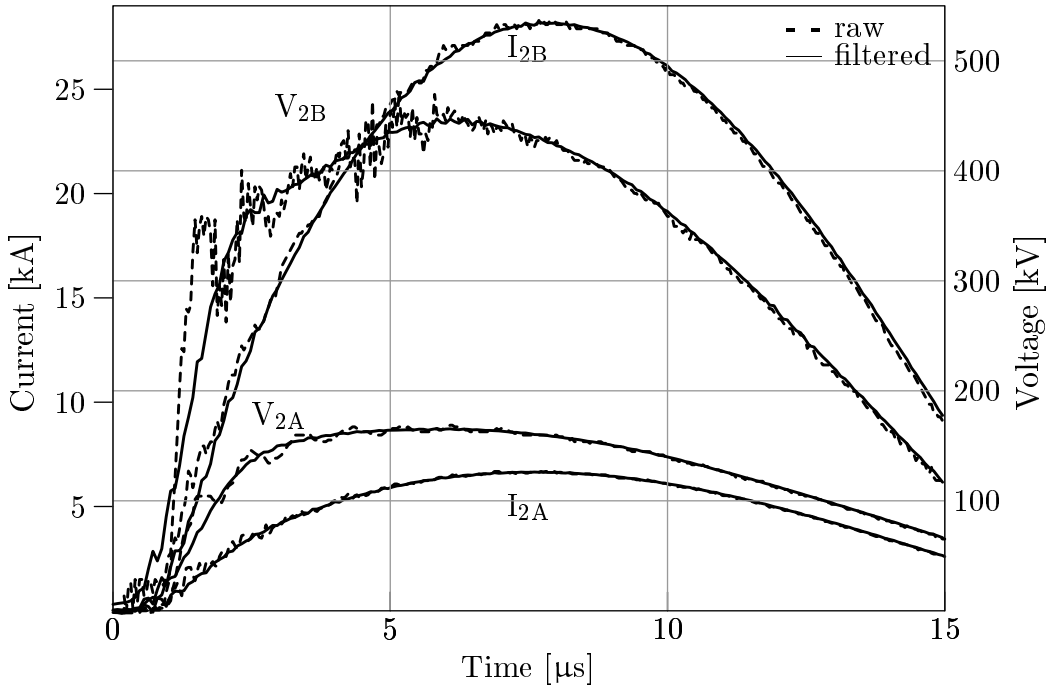

(a) Measured current and voltage.

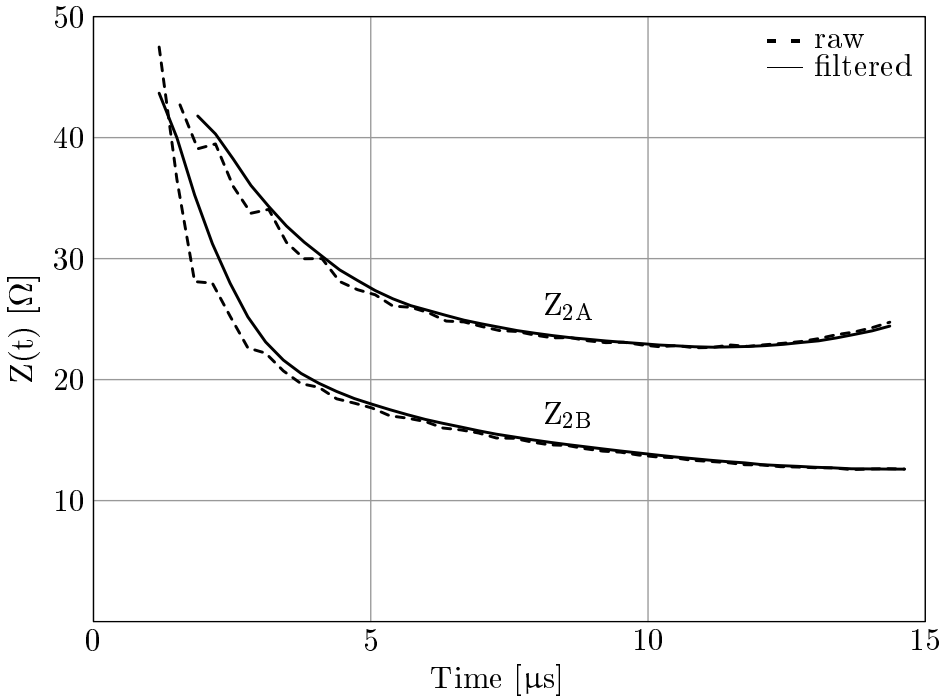

(b) Calculated dynamic impedance.

Figure C.8: Raw (dashed line) and filtered (solid line) experiment data for current waveshape 2 – 6/14 µs, 7 kA and 29 kA.

C.6 Conclusion

The inadvertent resonance discovered in the setup was found to be caused by the components and geometry of the experiment setup. This resonance manifested itself as an inductive ringing and was particularly evident on the front of the voltage measurements. It was necessary to filter the measurements to remove this noise using a band-stop filter. The final filtered experiment data enabled better calculation of the dynamic impedance data used in the thesis.

References

Anderson, R. B. & Eriksson, A. J. (1980), 'Lightning parameters for engineering application', *Electra*, no. 69, pp. 65–102.

Bellaschi, P. L., Armington, R. E. & Snowden, A. E. (1942), 'Impulse and 60-cycle characteristics of driven grounds – part II', *AIEE Transactions*, vol. 61, pp. 349–363.

Chisholm, W. A. & Janischewskyj, W. (1989), 'Lightning surge response of ground electrodes', *IEEE Transactions Power Delivery*, vol. 4, no. 2, pp. 1329–1337.

Chow, Y. L., Yang, J. J. & Srivastava, K. D. (1995), 'Grounding resistance of buried electrodes in multi-layer earth predicted by simple voltage measurements along earth surface - a theoretical discussion', *IEEE Transactions Power Delivery*, vol. 10, no. 2, pp. 707–715.

CIGRÉ WG 13:01 (1993), 'Applications of black box modeling to circuit breakers', *Electra*, no. 139, pp. 31–71.

CIGRE WG 33:01 (1991), 'Guide to procedures for estimating the lightning performance of transmission lines', WG 01 (Lightning) of Study Committee 33 (Overvoltages and Insulation Co–ordination).

Dawalibi, F. & Mukhedkar, D. (1974), 'Ground electrode resistance measurements in non uniform soils', *IEEE Transactions Power Apparatus and Systems*, vol. PAS-93, no. 1, pp. 109–115.

Dawalibi, F. P., Xiong, W. & Ma, J. (1995), 'Transient performance of substation structures and associated grounding systems', *IEEE Transactions on Industry Applications*, vol. 31, no. 3, pp. 520–527.

Dubé, L. (1996), 'Users guide to Models in ATP'.

Erler, J. W. & Snowden, D. P. (1983), 'High resolution studies of the electrical breakdown of soil', *IEEE Transactions on Nuclear Science*, vol. NS-30, no. 6, pp. 4564–4567.

Geri, A. (1999), 'Behaviour of grounding systems excited by high impulse currents: the model and its validation', *IEEE Transactions Power Delivery*, vol. 14, no. 3, pp. 1008–1017.

Geri, A. & Veca, G. M. (1994), Effects of lightning current on transmission line groundings, *in* '22nd International Conference on Lightning Protection', Budapest, Hungary.

Geri, A., Veca, G. M., Garbagnati, E. & Sartorio, G. (1992), 'Non-linear behaviour of ground electrodes under lightning surge currents: Computer modelling and comparison with experimental results', *IEEE Transactions on Magnetics*, vol. 28, no. 2, pp. 1442–1445.

Grant, M. D. & Nixon, K. J. (2006), Design of a re-usable rocket for triggered-lightning experiments, *in* '28th International Conference on Lightning Protection', Kanazawa, Japan. Accepted for publication: Abstract No. 1363.

Grant, M. D., Garrard, J. & Nixon, K. J. (2006), Low cost electric-field mill: Design, construction and testing, *in* 'Proceedings of the 15th Southern African Universities Power Engineering Conference', Durban, South Africa.

Grover, F. W. (1962), *Inductance Calculations : Working formulas and tables*, Dover Publications, Inc., New York.

Gunther, E. (1993), 'Running EMTP on PCs', *IEEE Computer Applications in Power*, pp. 33–38.

Hayashi, M. (1967), 'Observation of streamer in the soil by surge current [in Japanese]', *IEEJ Transactions on Power Systems and Energy*, vol. 87, no. 1, pp. 133–141.

IEC 60060–1 (1989), 'High-voltage test techniques. Part 1: General definitions and test requirements', IEC, Geneva.

IEEE Std 80 (2000), 'Guide for safety in AC substation grounding'. ISBN 0–7381–1926–1.

IEEE Std 81.2 (1991), 'Guide for for measurement of impedance and safety characteristics of large, extended or interconnected grounding systems'. ISBN 1–55937-187–0.

Korsuncev, A. V. (1958), 'Application on the theory of similarity to calculation of impulse characteristics of concentrated electrodes', *Elektrichestvo*, no. 5, pp. 31–35.

Kosztaluk, R., Łoboda, M. & Mukhedkar, D. (1981), 'Experimental study of transient ground impedances', *IEEE Transactions Power Apparatus and Systems*, vol. PAS-100, no. 11, pp. 4652–4660.

Kuffel, E., Zaengl, W. S. & Kuffel, J. (2000), *High Voltage Engineering: Fundamentals*, Newnes.

Leadon, R., Flanagan, T., Mallon, C. & Denson, R. (1983), 'Effect of ambient gas on arc initiation characteristics in soil', *IEEE Transactions on Nuclear Science*, vol. NS-30, no. 6, pp. 4572–4576.

Liew, A. C. & Darveniza, M. (1974), 'Dynamic model of impulse characteristics of concentrated earths', *Proceedings of the IEE*, vol. 121, no. 2, pp. 123–135.

Meyer, W. & Liu, T. (1982), *Electromagnetic Transients Program Rule Book*, Bonneville Power Administration.

Mousa, A. M. (1994), 'The soil ionization gradient associated with discharge of high currents into concentrated electrodes', *IEEE Transactions Power Delivery*, vol. 9, no. 3, pp. 1669–1677.

Nixon, K. J. (1999), Modelling the lightning transient response of an earth electrode system, Master's dissertation, University of the Witwatersrand, Johannesburg.

Nixon, K. J. & Jandrell, I. R. (2004*a*), Initial design of a system to determine the behaviour of an earth electrode subjected to real lightning discharges, *in* '27th International Conference on Lightning Protection', Avignon, France.

Nixon, K. J. & Jandrell, I. R. (2004*b*), 'Quantifying the lightning transient performance of an earth electrode', *Trans. of the SAIEE*, vol. 95, no. 1, pp. 18–23.

Nixon, K. J., Jandrell, I. R. & Phillips, A. J. (2005), Measuring the absolute transient voltage of a real earth electrode, *in* '14th International Symposium on High Voltage Engineering', Beijing, China.

Nixon, K. J., Jandrell, I. R. & Phillips, A. J. (2006), A simplified model of the lightning performance of a driven rod earth electrode in multi-layer soil that includes the effect of soil ionisation, *in* 'IEEE Industry Applications Society', 41st Annual Meeting, Florida, USA. Accepted for publication, Paper ID: IAS47p3.

Oettlé, E. E. (1987), The impulse impedance of concentrated earth electrodes, Master's dissertation, University of the Witwatersrand, Johannesburg.

Oettlé, E. E. (1988), 'A new general estimation curve for predicting the impulse impedance of concentrated earth electrodes', *IEEE Transactions Power Delivery*, vol. 3, pp. 2020–2029.

Pederson, D., Rohrer, R. & Nagel, L. (1989), 'Simulation Program with Integrated Circuit Emphasis (SPICE) Version 3f', University of California at Berkeley.

Petropoulos, G. M. (1948), 'The high-voltage characteristics of earth resistances', *IEE Journal*, vol. 95, no. 2, pp. 59–70.

Phillips, A. & Anderson, J. (2002), High current impulse testing of full-scale ground electrodes, Technical Report 1006866, EPRI, Palo Alto, California.

Phillips, A., Chisholm, W. & Anderson, J. (2004), Guide for transmission line grounding: a roadmap for design, testing and remediation, Technical Report 1002021, EPRI, Palo Alto, California.

Rakov, V. & Uman, M. (2003), *Lightning: Physics and effects*, Cambridge University Press. ISBN 0–521–58327–6.

SANS 10199 (2004), 'The design and installation of earth electrodes', South African National Standards, Pretoria. ISBN 0-626-15741-2.

SANS 10313 (1999), 'The protection of structures against lightning', South African National Standards, Pretoria. ISBN 0–626–12104–3.

Sekioka, S., Lorentzou, M. I., Philippakou, M. P. & Prousalidis, J. M. (2006), 'Current-dependent grounding resistance model based on energy balance of soil ionisation', *IEEE Transactions Power Delivery*, vol. 21, no. 1, pp. 194–201.

Snowden, D. P. & Erler, J. W. (1983), 'Initiation of electrical breakdown of soil by water vaporization', *IEEE Transactions on Nuclear Science*, vol. NS-30, no. 6, pp. 4568–4571.

Stearns, S. & David, R. (1988), *Signal Processing Algorithms*, Prentice-Hall, New Jersey.

Sunde, E. D. (1940), 'Surge characteristics of a buried wire', *AIEE Transactions*, vol. 59, pp. 987–991.

Sunde, E. D. (1949), *Earth Conduction Effects in Transmission Systems*, D. van Nostrand Company, Inc., New York.

Takahashi, T. & Kawase, T. (1990), 'Analysis of apparent resistivity in a multi-layer earth structure', *IEEE Transactions Power Delivery*, vol. 5, no. 2, pp. 604–612.

Towne, H. M. (1929), 'Impulse characteristics of driven grounds', *General Electric Review*, pp. 605–609.

Wang, J., Liew, A. C. & Darveniza, M. (2005), 'Extension of dynamic model of impulse behaviour of concentrated earths at high currents', *IEEE Transactions Power Delivery*, vol. 20, no. 3, pp. 2160–2165.

Yasuda, Y., Kondo, S., Hara, T., Ikeda, K., Sonoi, Y. & Furuoka, Y. (2003), 'Measurement of soil-ionization characteristics of grounding and its analysis using dynamic grounding model [in Japanese]', *IEEJ Transactions on Power Systems and Energy*, vol. 123-B, no. 6, pp. 718–724.

Bibliography

Almeida, M. E. & Correia de Barros, M. T. (1996), 'Accurate modelling of rod driven tower footing', *IEEE Transactions Power Delivery*, vol. 11, no. 3, pp. 1606–1609.

Ambelal, D. (1986), Earthing and grounding for the control of EMI in industrial instrumentation and control systems, Master's dissertation, University of the Witwatersrand, Johannesburg.

Ametani, A. (1976), 'A highly efficient method for calculating transmission line transients', *IEEE Transactions Power Apparatus and Systems*, vol. PAS-95, no. 5, pp. 1545–1551.

Amoruso, V. & Lattarulo, F. (1993), 'The electromagnetic field of an improved lightning return-stroke representation', *IEEE Transactions on Electromagnetic Compatibility*, vol. 35, no. 3, pp. 317–328.

Amoruso, V. & Lattarulo, F. (1994), 'Lightning-originated tangential electric field across air-soil interfaces', *IEE Proceedings on Science and Measurement Technology*, vol. 141, no. 1, pp. 65–70.

Anderson, J. G. (1982), *Transmission Line Reference Book 345 kV and Above*, 2nd edn, EPRI, Palo Alto, California, chapter 12 (Lightning Performance of Transmission Lines), pp. 544–597.

Anderson, R. B. & Eriksson, A. J. (1980), 'Lightning parameters for engineering application', *Electra*, no. 69, pp. 65–102.

Bellaschi, P. L. (1941), 'Impulse and 60-cycle characteristics of driven grounds', *AIEE Transactions*, vol. 60, pp. 122–132.

Bellaschi, P. L. & Armington, R. E. (1943), 'Impulse and 60-cycle characteristics of driven grounds – part III', *AIEE Transactions*, vol. 62, pp. 334–344.

Bellaschi, P. L., Armington, R. E. & Snowden, A. E. (1942), 'Impulse and 60-cycle characteristics of driven grounds – part II', *AIEE Transactions*, vol. 61, pp. 349–363.

Berger, K. (1946), 'Das verhalten von erdungen unter hohen stoßströmen', *Bull. Assoc. Suisse Elek*, no. 37, pp. 197–211.

Bewley, L. V. (1934), 'Theory and tests of the counterpoise', *Electrical Engineering*, vol. 53, pp. 1163–1172.

Bewley, L. V. (1963), *Travelling Waves on Transmission Lines*, 2nd edn, Dover Publications, Inc., New York.

Blattner, C. J. (1980), 'Prediction of soil resistivity and ground rod resistance for deep ground electrodes', *IEEE Transactions Power Apparatus and Systems*, vol. PAS-99, no. 5, pp. 1758–1763.

Card, R. H. (1935), 'Earth resistivity and geological structure', *Electrical Engineering*, vol. 54, pp. 1153–1161.

CDEGS (1996), 'Current Distribution, Electromagnetic interference, Grounding and Soil structure analysis', Computer Software, Safe Engineering Services and Technologies, Montréal.

Chisholm, W. A. & Janischewskyj, W. (1989), 'Lightning surge response of ground electrodes', *IEEE Transactions Power Delivery*, vol. 4, no. 2, pp. 1329–1337.

Chow, Y. L., Elsherbiny, M. M. & Salama, M. M. A. (1996), 'Resistance formulas of grounding systems in two-layer earth', *IEEE Transactions Power Delivery*, vol. 11, no. 3, pp. 1330–1336.

Chow, Y. L., Yang, J. J. & Srivastava, K. D. (1995), 'Grounding resistance of buried electrodes in multi-layer earth predicted by simple voltage measurements along earth surface - a theoretical discussion', *IEEE Transactions Power Delivery*, vol. 10, no. 2, pp. 707–715.

CIGRÉ WG 13:01 (1993), 'Applications of black box modeling to circuit breakers', *Electra*, no. 139, pp. 31–71.

CIGRE WG 33:01 (1991), 'Guide to procedures for estimating the lightning performance of transmission lines', WG 01 (Lightning) of Study Committee 33 (Overvoltages and Insulation Co–ordination).

CIGRÉ WG 33:01 (1995), 'Updates to lightning current waveforms', *Electra*, no. 161, pp. 83.

Cristina, S. & Oriandi, A. (1991), Circuit modeling for lightning protection systems : EMI evaluation in presence of the lightning channel, *in* '7th International Symposium on High Voltage Engineering', Dresden, Germany, pp. 73–76.

Daily, W. K. & Dawalibi, F. (1994), 'Measurements and computations of electromagnetic fields in electric power substations', *IEEE Transactions Power Delivery*, vol. 9, no. 1, pp. 324–333.

Davies, A. M., Griffiths, H. & Charlton, T. E. (1998), High frequency performance of a vertical earth rod, *in* '24th International Conference on Lightning Protection', Birmingham, U.K., pp. 536–540.

Dawalibi, F. & Finney, W. G. (1980), 'Transmission line tower grounding performance in non-uniform soil', *IEEE Transactions Power Apparatus and Systems*, vol. PAS-99, no. 2, pp. 471–479.

Dawalibi, F. & Mukhedkar, D. (1974), 'Ground electrode resistance measurements in non uniform soils', *IEEE Transactions Power Apparatus and Systems*, vol. PAS-93, no. 1, pp. 109–115.

Dawalibi, F. & Mukhedkar, D. (1975*a*), 'Optimum design of substation grounding in a two layer earth structure (part I) – Analytical study', *IEEE Transactions Power Apparatus and Systems*, vol. PAS-94, no. 2, pp. 252–261.

Dawalibi, F. & Mukhedkar, D. (1975*b*), 'Optimum design of substation grounding in a two layer earth structure (part II) – Comparison', *IEEE Transactions Power Apparatus and Systems*, vol. PAS-94, no. 2, pp. 262–272.

Dawalibi, F. & Mukhedkar, D. (1975*c*), 'Optimum design of substation grounding in a two layer earth structure (part III) – Study of grounding grids performance and new electrodes configuration', *IEEE Transactions Power Apparatus and Systems*, vol. PAS-94, no. 2, pp. 267–272.

Dawalibi, F. P., Xiong, W. & Ma, J. (1995), 'Transient performance of substation structures and associated grounding systems', *IEEE Transactions on Industry Applications*, vol. 31, no. 3, pp. 520–527.

Dénommé, F., Trinh, B. G. & Mukhedkar, D. (1973), 'Transient response of a floor net used as a ground return in high voltage test areas', *IEEE Transactions Power Apparatus and Systems*, vol. PAS-92, no. 6, pp. 2007–2014.

Devgan, S. S. & Whitehead, E. R. (1973), 'Analytical models for distributed grounding systems', *Proceedings of the IEEE*, vol. 92, no. 5, pp. 1763–1770.

Dommel, H. W. & Meyer, W. S. (1974), 'Computation of electromagnetic transients', *Proceedings of the IEEE*, vol. 62, no. 7, pp. 983–993.

Dubé, L. (1996), 'Users guide to Models in ATP'.

Dwight, H. B. (1936), 'Calculation of resistance to ground', *Electrical Engineering*, vol. 55, pp. 1319–1328.

Eaton, J. R. (1941*a*), 'Grounding electric circuits effectively – Part I : Characteristics of grounds', *General Electric Review*, vol. 44, no. 6, pp. 323–327.

Eaton, J. R. (1941*b*), 'Grounding electric circuits effectively – Part II : Calculations and installation', *General Electric Review*, vol. 44, no. 7, pp. 397–404.

Eaton, J. R. (1941*c*), 'Grounding electric circuits effectively – Part III : Ground system requirements', *General Electric Review*, vol. 44, no. 8, pp. 451–456.

Eaton, J. R. (1944), 'Impulse characteristics of electrical connections to the earth', *General Electric Review*, vol. 47, no. 10, pp. 41–50.

Erler, J. W. & Snowden, D. P. (1983), 'High resolution studies of the electrical breakdown of soil', *IEEE Transactions on Nuclear Science*, vol. NS-30, no. 6, pp. 4564–4567.

Eytani, D. M. (1995), Earthing electrodes - power frequency and impulse behaviour, Master's dissertation, University of the Witwatersrand, Johannesburg.

Fawssett, E., Grimmitt, H. W., Shotter, G. F. & Taylor, H. G. (1940), 'Practical aspects of earthing', *IEE Journal*, vol. 87, no. 526, pp. 357–400.

Flisowski, Z., Stańczak, B., Kuca, B., C.Mazzetti, Orlandi, A. & Yarmarkin, M. (1996), Induced currents and voltages inside LPS models due to lightning current, *in* '23rd International Conference on Lightning Protection', Firenze, Italy, pp. 527–532.

Gallagher, T. J. & Pearmain, A. J. (1983), *High Voltage Measurement, Testing and Design*, John Wiley and Sons, chapter 3 (Field Plotting), pp. 76–93.

Geldenhuys, H. J. (1995), The Effects of Lightning in Shallow Coal Mines - An Engineering Study, PhD thesis, University of the Witwatersrand, Johannesburg.

Geldenhuys, H. J., Eriksson, A. J. & Bourne, G. W. (1989), 'Fifteen years' data of lightning current measurements on a 60 m mast', *Trans. of the SAIEE*, pp. 98–103.

Geri, A. (1999), 'Behaviour of grounding systems excited by high impulse currents: the model and its validation', *IEEE Transactions Power Delivery*, vol. 14, no. 3, pp. 1008–1017.

Geri, A. & Veca, G. M. (1994), Effects of lightning current on transmission line groundings, *in* '22nd International Conference on Lightning Protection', Budapest, Hungary.

Geri, A., Veca, G. M., Garbagnati, E. & Sartorio, G. (1992), 'Non-linear behaviour of ground electrodes under lightning surge currents: Computer modelling and comparison with experimental results', *IEEE Transactions on Magnetics*, vol. 28, no. 2, pp. 1442–1445.

Golde, ed. (1977), *Lightning - Vol. 2*, Academic Press, London, chapter 18 - Lightning Earths - E. K. Saraoja, pp. 577–598.

Grant, M. D. & Nixon, K. J. (2006), Design of a re-usable rocket for triggered-lightning experiments, *in* '28th International Conference on Lightning Protection', Kanazawa, Japan. Accepted for publication: Abstract No. 1363.

Grant, M. D., Garrard, J. & Nixon, K. J. (2006), Low cost electric-field mill: Design, construction and testing, *in* 'Proceedings of the 15th Southern African Universities Power Engineering Conference', Durban, South Africa.

Grcev, L. (1991), Frequency dependent analysis of electric field distribution of grounding systems, *in* '7th International Symposium on High Voltage Engineering', Dresden, Germany, pp. 155–158.

Grcev, L. (1992), Numerical analysis of the transient voltages near grounding systems, *in* '21st International Conference on Lightning Protection', Berlin, Germany, pp. 105–110.

Grcev, L. (1994), Analysis of the possibility of soil breakdown due to lightning in complex and spacious grounding systems, *in* '22nd International Conference on Lightning Protection', Budapest, Hungary.

Grcev, L. & Dawalibi, F. (1990), 'An electromagnetic model for transients in grounding systems', *IEEE Transactions Power Delivery*, vol. 5, no. 4, pp. 1773–1781.

Grcev, L. D. & Heimbach, M. (1996), Computer simulation of transient ground potential rise in large earthing systems, *in* '23rd International Conference on Lightning Protection', Firenze, Italy, pp. 585–590.

Grcev, L. D. & Menter, F. E. (1996), 'Calculating the impedance of a grounding system', *IEEE Transactions on Magnetics*, vol. 32, no. 3, pp. 1525–1528.

Grover, F. W. (1962), *Inductance Calculations : Working formulas and tables*, Dover Publications, Inc., New York.

Gunther, E. (1993), 'Running EMTP on PCs', *IEEE Computer Applications in Power*, pp. 33–38.

Gupta, B. R. & Thapar, B. (1980), 'Impulse impedance of grounding grids', *IEEE Transactions Power Apparatus and Systems*, vol. PAS-99, no. 6, pp. 2357–2362.

Hayashi, M. (1967), 'Observation of streamer in the soil by surge current [in Japanese]', *IEEJ Transactions on Power Systems and Energy*, vol. 87, no. 1, pp. 133–141.

Heidler, F., Zischank, W., Wiesinger, J., Kern, A. & Seevers, M. (1998), Induced overvoltages in cable ducts taking into account the current flow into earth, *in* '24th International Conference on Lightning Protection', Birmingham, U.K., pp. 270–275.

Heimbach, M. & Grcev, L. (1997), Simulation of grounding structures within EMTP, *in* '10th International Symposium on High Voltage Engineering', Vol. 5, Montréal, Québec, Canada, pp. 131–135.

Hemstreet, J. G., Lewis, W. W. & Foust, C. M. (1942), 'Study of driven rods and counterpoise wires in high-resistance soil on consumers power company 140 kV system', *AIEE Transactions*, vol. 61, pp. 628–633.

Howard Wise, W. (1948), 'Potential coefficients for ground return circuits', *Bell System Technical Journal*, vol. 27, pp. 365–371.

Huang, L. & Chen, X. (1993), 'Study of unequally spaced grounding grids', *IEEE Transactions Power Delivery*, vol. 10, no. 2, pp. 716–722.

IEC 60060–1 (1989), 'High-voltage test techniques. Part 1: General definitions and test requirements', IEC, Geneva.

IEEE Std 80 (2000), 'Guide for safety in AC substation grounding'. ISBN 0–7381–1926–1.

IEEE Std 81.2 (1991), 'Guide for for measurement of impedance and safety characteristics of large, extended or interconnected grounding systems'. ISBN 1–55937-187–0.

Kalat, W., Łoboda, M. & Pochanke, Z. (1994), Implementation of the dynamic model of surge soil conduction for transient behaviour of grounding electrodes simulations using ATP version of EMTP, *in* '22nd International Conference on Lightning Protection', Budapest, Hungary.

Karaki, S., Yamazaki, T., Nojima, K., Yokota, T., Murase, H., Takahashi, H. & Kojima, S. (1995), 'Transient impedance of GIS grounding grid', *IEEE Transactions Power Delivery*, vol. 10, no. 2, pp. 723–731.

Kern, A., Wiesinger, J. & Zischank, W. (1991), Calculation of the longitudinal voltage along metal tubes caused by lightning currents and protection measures, *in* '7th International Symposium on High Voltage Engineering', Dresden, Germany, pp. 147–150.

Khalifa, M., ed. (1990), *High-Voltage Engineering Theory and Practice*, Marcel Dekker, Inc., New York, chapter 13 (Grounding Systems), A. El-Morshedy, pp. 331–355.

Korsuncev, A. V. (1958), 'Application on the theory of similarity to calculation of impulse characteristics of concentrated electrodes', *Elektrichestvo*, no. 5, pp. 31–35.

Kosztaluk, R., Łoboda, M. & Mukhedkar, D. (1981), 'Experimental study of transient ground impedances', *IEEE Transactions Power Apparatus and Systems*, vol. PAS-100, no. 11, pp. 4652–4660.

Kraus, J. D. (1991), *Electromagnetics*, 4th edn, McGraw-Hill, International Edition.

Kuffel, E., Zaengl, W. S. & Kuffel, J. (2000), *High Voltage Engineering: Fundamentals*, Newnes.

Lagacé, P. J., Fortin, J. & Crainic, E. D. (1996), 'Interpretation of resistivity sounding measurements in n-layer soil using electrostatic images', *IEEE Transactions Power Delivery*, vol. 11, no. 3, pp. 1349–1354.

Lagacé, P. J., Houle, J. L., Gervais, Y. & Mukhedkar, D. (1988), 'Evaluation of the voltage distribution around toroidal HVDC ground electrodes in n-layer soils', *IEEE Transactions Power Delivery*, vol. 3, no. 4, pp. 1573–1579.

Leadon, R., Flanagan, T., Mallon, C. & Denson, R. (1983), 'Effect of ambient gas on arc initiation characteristics in soil', *IEEE Transactions on Nuclear Science*, vol. NS-30, no. 6, pp. 4572–4576.

Liew, A. C. & Darveniza, M. (1974), 'Dynamic model of impulse characteristics of concentrated earths', *Proceedings of the IEE*, vol. 121, no. 2, pp. 123–135.

Ljung, L. & Glad, T. (1994), *Modelling of Dynamic Systems*, Prentice Hall.

Łoboda, M. & Scuka, V. (1996), On the transient characteristics of electrical discharges and ionisation processes in soil, *in* '23rd International Conference on Lightning Protection', Firenze, Italy, pp. 539–544.

Long, W., Cotcher, D., Ruiu, D., Adam, P., Lee, S. & Adapa, R. (1990), 'EMTP - a powerful tool for analyzing power system transients', *IEEE Computer Applications in Power*, pp. 36–41.

Marti, J. R. (1982), 'Accurate modelling of frequency-dependent transmission lines in electromagnetic transient simulations', *IEEE Transactions Power Apparatus and Systems*, vol. PAS-101, no. 1, pp. 147–155.

Matsui, T., Adachi, M., Fukuzono, F., Sekioka, S., Yamamoto, O. & Hara, T. (1997), Measurements of grounding resistances of a transmission-line tower base connected with auxillary grounding electrodes for high impulse currents, *in* '10th International Symposium on High Voltage Engineering', Vol. 5, Montréal, Québec, Canada, pp. 257–260.

Mazzetti, C. & Veca, G. M. (1983), 'Impulse behaviour of ground electrodes', *IEEE Transactions Power Apparatus and Systems*, vol. PAS-102, no. 9, pp. 3148–3156.

Meliopoulos, A. P. & Moharam, M. G. (1983), 'Transient analysis of grounding systems', *IEEE Transactions Power Apparatus and Systems*, vol. PAS-102, no. 2, pp. 389–399.

Meliopoulos, A. P. S., Xia, F., Joy, E. B. & Cokkinides, G. J. (1993), 'An advanced computer model for grounding system analysis', *IEEE Transactions Power Delivery*, vol. 8, no. 1, pp. 13–23.

Meliopoulos, A. P., Webb, R. P. & Joy, E. B. (1981), 'Analysis of grounding systems', *IEEE Transactions Power Apparatus and Systems*, vol. PAS-100, no. 3, pp. 1039–1048.

Menter, F. (1991), Propagation of electrical transients along extended, imperfectly grounded structures, *in* '7th International Symposium on High Voltage Engineering', Dresden, Germany, pp. 171–174.

Menter, F. (1992), Transient analysis of earthing systems, *in* '21st International Conference on Lightning Protection', Berlin, Germany, pp. 87–92.

Menter, F. E. & Grcev, L. (1994), 'EMTP-based model for grounding system analysis', *IEEE Transactions Power Delivery*, vol. 9, no. 4, pp. 1838–1849.

Meyer, W. & Liu, T. (1982), *Electromagnetic Transients Program Rule Book*, Bonneville Power Administration.

Ming, Y., Scuka, V. & Lövstrand, K.-G. (1994), Earthing mechanism for an electrical system in sea water, *in* '22nd International Conference on Lightning Protection', Budapest, Hungary.

Mitani, H. (1980), 'Magnitude and frequency of transient induced voltages in low-voltage control circuits of power stations and substations', *IEEE Transactions Power Apparatus and Systems*, vol. PAS-99, no. 5, pp. 1871–1878.

Moore, R. J. C. (1980*a*), High voltage system earthing general principles - part one, Technical Report 123/2/128, Eskom Electrical Research.

Moore, R. J. C. (1980*b*), High voltage system earthing general principles - part two, Technical Report 123/2/128.1, Eskom Electrical Research.

Mousa, A. M. (1994), 'The soil ionization gradient associated with discharge of high currents into concentrated electrodes', *IEEE Transactions Power Delivery*, vol. 9, no. 3, pp. 1669–1677.

Mukhedkar, D., Gervais, Y. & Dawalibi, F. (1973*a*), 'Modelling of potential distribution around a grounding electrode', *IEEE Transactions Power Apparatus and Systems*, vol. PAS-92, no. 6, pp. 1455–1459.

Mukhedkar, D., Gervais, Y. & DeJean, J.-P. (1973*b*), 'Modelling of a grounding electrode', *IEEE Transactions Power Apparatus and Systems*, vol. PAS-92, no. 1, pp. 295–297.

Nahman, J. M. & Djordjevic, V. B. (1996), 'Resistance to ground of combined grid – multiple rods electrodes', *IEEE Transactions Power Delivery*, vol. 11, no. 3, pp. 1337–1342.

Nahman, J. M. & Salamon, D. D. (1988), 'A practical method for the interpretation of earth resistivity data obtained from driven rod tests', *IEEE Transactions Power Delivery*, vol. 3, no. 4, pp. 1375–1379.

Nahman, J. M., Djordjevic, V. B. & Salamon, D. D. (1996), 'Nonuniformity correction factors for maximum mesh-voltages of combined grid - multiple rods electrodes', *IEEE Transactions Power Delivery*, vol. 11, no. 3, pp. 1343–1348.

Nekhoul, B., Labie, P., Zgainski, F. X. & Meunier, G. (1996), 'Calculating the impedance of a grounding system', *IEEE Transactions on Magnetics*, vol. 32, no. 3, pp. 1509–1512.

Ng, H. W. (1996), Efficient and economic grounding arrangements for distribution lines, Technical Report TR-105907, EPRI.

Nixon, K. J. (1999), Modelling the lightning transient response of an earth electrode system, Master's dissertation, University of the Witwatersrand, Johannesburg.

Nixon, K. J. & Jandrell, I. R. (2004*a*), Initial design of a system to determine the behaviour of an earth electrode subjected to real lightning discharges, *in* '27th International Conference on Lightning Protection', Avignon, France.

Nixon, K. J. & Jandrell, I. R. (2004*b*), 'Quantifying the lightning transient performance of an earth electrode', *Trans. of the SAIEE*, vol. 95, no. 1, pp. 18–23.

Nixon, K. J. & Jandrell, I. R. (2005), Proposal for a simplified model of the transient behaviour of a single vertical earth rod in multi-layer soil, *in* 'Proceedings of the 14th Southern African Universities Power Engineering Conference', Johannesburg, South Africa.

Nixon, K. J., Jandrell, I. R. & Phillips, A. J. (2005), Measuring the absolute transient voltage of a real earth electrode, *in* '14th International Symposium on High Voltage Engineering', Beijing, China.

Nixon, K. J., Jandrell, I. R. & Phillips, A. J. (2006), A simplified model of the lightning performance of a driven rod earth electrode in multi-layer soil that includes the effect of soil ionisation, *in* 'IEEE Industry Applications Society', 41st Annual Meeting, Florida, USA. Accepted for publication, Paper ID: IAS47p3.

Nixon, K. J., Jandrell, I. R. & Van Coller, J. M. (1998*a*), Development of earth electrode models suitable for South African conditions, *in* '24th International Conference on Lightning Protection', Birmingham, U.K., pp. 550–555.

Nixon, K. J., Jandrell, I. R. & Van Coller, J. M. (1998*b*), Evaluation of modelling techniques used to study the transient performance of an earth electrode, *in* 'Proceedings of the 7th Southern African Universities Power Engineering Conference', Stellenbosch, South Africa.

Nixon, K. J., Jandrell, I. R. & Van Coller, J. M. (1999*a*), Consideration of the relative effect of soil ionisation and mutual interaction of components on the partial lightning current distribution in earth electrode systems, *in* '11th International Symposium on High Voltage Engineering', Vol. 2, London, UK, pp. 284–287. ISBN 0–85296–719–5.

Nixon, K. J., Jandrell, I. R. & Van Coller, J. M. (1999*b*), Modelling earth electrodes under transient conditions, *in* 'Joint Colloquium of SAIEE and CIGRÉ Study Committee 36: Interference in Power Systems: Low Frequency and High Frequency', Midrand, South Africa.

Nixon, K. J., Jandrell, I. R. & Van Coller, J. M. (1999*c*), A preliminary consideration of the effects of mutual interaction between components on the performance

of an earth electrode system subjected to a lightning transient current, *in* 'Proceedings of the 8th Southern African Universities Power Engineering Conference', Potchefstroom, South Africa. ISBN 1–86822–344–2.

Oettlé, E. E. (1987), The impulse impedance of concentrated earth electrodes, Master's dissertation, University of the Witwatersrand, Johannesburg.

Oettlé, E. E. (1988*a*), 'The characteristics of electrical breakdown and ionization processes in soil', *Trans. of the SAIEE*, vol. 79, no. 2, pp. 63–70.

Oettlé, E. E. (1988*b*), 'A new general estimation curve for predicting the impulse impedance of concentrated earth electrodes', *IEEE Transactions Power Delivery*, vol. 3, pp. 2020–2029.

Oettlé, E. E. (1988*c*), 'Results of impulse tests on practical electrodes at the high-voltage laboratory of the national electrical engineering research institute', *Trans. of the SAIEE*, vol. 79, no. 2, pp. 71–78.

Papalexopoulos, A. D. & Meliopoulos, A. P. (1987), 'Frequency dependent characteristics of grounding systems', *IEEE Transactions Power Delivery*, vol. 2, no. 4, pp. 1073–1081.

Pederson, D., Rohrer, R. & Nagel, L. (1989), 'Simulation Program with Integrated Circuit Emphasis (SPICE) Version 3f', University of California at Berkeley.

Petropoulos, G. M. (1948), 'The high-voltage characteristics of earth resistances', *IEE Journal*, vol. 95, no. 2, pp. 59–70.

Phillips, A. & Anderson, J. (2002), High current impulse testing of full-scale ground electrodes, Technical Report 1006866, EPRI, Palo Alto, California.

Phillips, A., Chisholm, W. & Anderson, J. (2004), Guide for transmission line grounding: a roadmap for design, testing and remediation, Technical Report 1002021, EPRI, Palo Alto, California.

Phillips, A. J., Grobbelaar, G. B., Pritchard, C. J., Melaia, R. & Jandrell, I. R. (1996), 'Development of a Rogowski coil to measure lightning current impulses', *Trans. of the SAIEE*.

Phillips, A., White, P. & J. Anderson, K. K. (2002), Tower grounding and soil ionization report, Technical Report 1001908, EPRI, Palo Alto, California.

Popović, L. M. (1988), 'Potential distribution along external electrodes of a high voltage installation grounding system', *IEEE Transactions Power Delivery*, vol. 3, no. 4, pp. 1580–1587.

Rakov, V. & Uman, M. (2003), *Lightning: Physics and effects*, Cambridge University Press. ISBN 0–521–58327–6.

Rančić, P. D., Stajić, Z. P., Tošić, B. S. & Djordjević, D. R. (1996), 'Analysis of linear ground electrodes placed in vertical three-layer earth', *IEEE Transactions on Magnetics*, vol. 32, no. 3, pp. 1505–1508.

Rüdenberg, R. (1945), 'Grounding principles and practice (part 1) – Fundemental considerations on grounding currents', *Electrical Engineering*, vol. 64, pp. 1–13.

Rüdenburg, R. (1968), *Electrical Shock Waves in Power Systems (Electrische Wanderwellen translated by H. J. Wetzstein)*, Harvard University Press, Cambridge, Massachusetts.

SABS IEC 61312–1 (1995), 'Protection against lightning electromagnetic impulse', IEC, Geneva, (South African National Standards, Pretoria). ISBN 0–626–10627–3.

SANS 10199 (2004), 'The design and installation of earth electrodes', South African National Standards, Pretoria. ISBN 0-626-15741-2.

SANS 10313 (1999), 'The protection of structures against lightning', South African National Standards, Pretoria. ISBN 0–626–12104–3.

SANS IEC 61024–1 (1990), 'Protection of structures against lightning: Part 1 : General principles', IEC, Geneva, (South African National Standards, Pretoria). ISBN 0–626–10223–5.

Sekioka, S., Lorentzou, M. I., Philippakou, M. P. & Prousalidis, J. M. (2006), 'Current-dependent grounding resistance model based on energy balance of soil ionisation', *IEEE Transactions Power Delivery*, vol. 21, no. 1, pp. 194–201.

Snowden, D. P. & Erler, J. W. (1983), 'Initiation of electrical breakdown of soil by water vaporization', *IEEE Transactions on Nuclear Science*, vol. NS-30, no. 6, pp. 4568–4571.

Spilkin, F. & Goldberg, N. (1965), *South African Earthing Principles*, Steam and Mining Equipment (Pty.) Ltd.

Stearns, S. & David, R. (1988), *Signal Processing Algorithms*, Prentice-Hall, New Jersey.

Sunde, E. D. (1936), 'Currents and potentials along leaky ground-return conductors', *Electrical Engineering*, vol. 55, pp. 1338–1346.

Sunde, E. D. (1940), 'Surge characteristics of a buried wire', *AIEE Transactions*, vol. 59, pp. 987–991.

Sunde, E. D. (1949), *Earth Conduction Effects in Transmission Systems*, D. van Nostrand Company, Inc., New York.

Tagg, G. F. (1964), *Earth Resistances*, George Newnes Ltd., London.

Takahashi, T. & Kawase, T. (1990), 'Analysis of apparent resistivity in a multi-layer earth structure', *IEEE Transactions Power Delivery*, vol. 5, no. 2, pp. 604–612.

Takashima, T., Nakae, T. & Ishibashi, R. (1981), 'High frequency characteristics of impedances to ground and field distributions of ground electrodes', *IEEE Transactions Power Apparatus and Systems*, vol. PAS-100, no. 4, pp. 1893–1900.

Thapar, B. & Gerez, V. (1995), 'Equivalent resistivity of non-uniform soil for grounding grid design', *IEEE Transactions Power Delivery*, vol. 10, no. 2, pp. 759–767.

Towne, H. M. (1929), 'Impulse characteristics of driven grounds', *General Electric Review*, pp. 605–609.

Trinh, G. N. & Maruvada, S. P. (1972), 'Effect of a two-layer earth on the electric field near ground electrodes', *IEEE Transactions Power Apparatus and Systems*, vol. PAS-91, no. 6, pp. 2356–2365.

Vainer, A. L. (1966), 'Impulse characteristics of complex earth grids', *Elektrichestvo*, no. 3, pp. 23–27.

Vainer, A. L. & Floru, V. N. (1971), 'Experimental study and method of calculation of the impulse characteristics of deep earthings', *Elektrichestvo*, no. 5, pp. 18–22.

Van Coller, J. M. & Jandrell, I. R. (1992), Behaviour of interconnected building earths under surge conditions, *in* '21st International Conference on Lightning Protection', Berlin, Germany.

van der Merwe, W. C. (1985), 765 kV line lightning performance and the implications for a gas insulated substation, Master's dissertation, University of the Witwatersrand, Johannesburg.

van der Westhuizen, C. (1980), High voltage system earthing - potential field plotting in an electrolytic tank, Technical Report 123/2/149, Eskom Electrical Research.

Velazquez, R. & Mukhedkar, D. (1984), 'Analytical modelling of grounding electrodes transient behaviour', *IEEE Transactions Power Apparatus and Systems*, vol. 103, pp. 1314–1322.

Verma, R. & Mukhedkar, D. (1980), 'Impulse impedance of buried ground wire', *IEEE Transactions Power Apparatus and Systems*, vol. PAS-99, no. 5, pp. 2003–2007.

Verma, R. & Mukhedkar, D. (1981), 'Fundamental considerations and impulse impedance of grounding grids', *IEEE Transactions Power Apparatus and Systems*, vol. PAS-100, no. 3, pp. 1023–1030.

Visacro, S. F. & Portela, C. M. (1992), Modelling of earthing systems for lightning protection applications, including propagation effects, *in* '21st International Conference on Lightning Protection', Berlin, Germany, pp. 129–132.

Visacro, S. F. & Portela, C. M. (1994), Sensitivity analysis for the effect of lightning current intensity on the behaviour of earthing systems, *in* '22nd International Conference on Lightning Protection', Budapest, Hungary.

Visacro, S. F. & Soares, A. J. (1996), Simplified models for tower-footing grounding of transmission lines for evaluation of lightning performance, *in* '23rd International Conference on Lightning Protection', Firenze, Italy, pp. 574–578.

Wang, J., Liew, A. C. & Darveniza, M. (2005), 'Extension of dynamic model of impulse behaviour of concentrated earths at high currents', *IEEE Transactions Power Delivery*, vol. 20, no. 3, pp. 2160–2165.

Yasuda, Y., Hirakawa, Y., Shiraishi, K. & Hara, T. (2001), 'Sensitivity analysis on grounding models for 500 kV transmission lines', *IEEJ Transactions on Power Systems and Energy*, vol. 121-B, no. 10, pp. 1386–1393.

Yasuda, Y., Kondo, S., Hara, T., Ikeda, K., Sonoi, Y. & Furuoka, Y. (2003*a*), 'Lightning surge analysis for 500 kV transmission lines using grounding model with dynamic characteristics [in Japanese]', *IEEJ Transactions on Power Systems and Energy*, vol. 123-B, no. 2, pp. 245–251.

Yasuda, Y., Kondo, S., Hara, T., Ikeda, K., Sonoi, Y. & Furuoka, Y. (2003*b*), 'Measurement of soil-ionization characteristics of grounding and its analysis using dynamic grounding model [in Japanese]', *IEEJ Transactions on Power Systems and Energy*, vol. 123-B, no. 6, pp. 718–724.

Zaborosky, J. (1955), 'Efficiency of grounding grids with non-uniform soil', *AIEE Transactions*, vol. 74, no. III (Power Apparatus and Systems), pp. 1230–1233.